TAMPEREEN TEKNILLINEN YLIOPISTO
TAMPERE UNIVERSITY OF TECHNOLOGY
Julkaisu 801 • Publication 801

Marju Ferenets

Functional Optical Fibers – Organic and Hybrid Structures

Tampere 2009

Tampereen teknillinen yliopisto. Julkaisu 801
Tampere University of Technology. Publication 801

Marju Ferenets

Functional Optical Fibers – Organic and Hybrid Structures

Thesis for the degree of Doctor of Technology to be presented with due permission for public examination and criticism in Tietotalo Building, Auditorium TB111, at Tampere University of Technology, on the 24th of April 2009, at 12 noon.

Tampereen teknillinen yliopisto - Tampere University of Technology
Tampere 2009

ISBN 978-952-15-2139-3 (printed)
ISBN 978-952-15-2146-1 (PDF)
ISSN 1459-2045

Functional Optical Fibers—Organic and Hybrid Structures

Marju Ferenets

April 8, 2009

You can know the name of a bird in all the languages of the world, but when you're finished, you'll know absolutely nothing whatever about the bird... So let's look at the bird and see what it's doing – that's what counts. I learned very early the difference between knowing the name of something and knowing something.

Richard P. Feynman

Abstract

Constant need for saving space and energy has led to the miniaturization of electronic devices and to the integration of such devices into various unconventional substrates like different kind of fibers. It has been proposed and in some cases already demonstrated that electronic devices such as light emitting diodes, photovoltaic cells, thin film transistors could be deposited straight to the fibers. Traditional textile fibers do not offer sufficiently stable and smooth base for electronic devices. Plastic optical fibers (POF) that are flexible and of small size are suitable candidates for functional fibers and can be easily incorporated into the textile structure. POF could also enable to use light as an information carrier instead of typical electrical signals and would provide interesting lighting solutions.

Such fibrous electronic devices however need new type of materials thats processing techniques would be compatible with cylindrical shape of the substrate and could be processable at temperatures suitable for plastic fibers. Inherently conductive polymers (ICPs) have opened the way to polymeric electronics thats driving force is the manufacturing of electronics at low cost on flexible substrates using solution processing methods such as printing or dip-coating. For some device components one has to still use inorganic materials that have nowadays been developed in a form compatible with plastic substrates and their processing conditions (e.g. indium tin oxide in a form of printing ink).

The aim of this thesis is to study possibilities to combine unique properties of POF and ICPs in a form of functional optical fibers. This goal is realized by first studying manufacturing methods of POF as a substrate of functional fibers. In the second step of the research two different ICPs—polypyrrole (PPy) and poly(3,4-ethylene dioxythiophene) (PEDOT)—are studied as components of possible electronic devices. PPy films in a planar and fiber form are studied for transparent electrode application. Film formation is successful, but the results suggest that

such PPy films have insufficient electrical conductivity and environmental stability for any real electronic device applications.

PEDOT films are studied for ammonia sensor application in electrical and optical regime. It is demonstrated that PEDOT films can be used for detecting gaseous ammonia. Comparative study between the sensitivity of PEDOT:*p*-toluene sulfonate (PTS) and films made of commercially available aqueous dispersion of PEDOT:poly(styrene sulfonate) indicates that *in situ* polymerized PEDOT:PTS has better performance in sensor application due to its smaller counter-ion and larger surface area.

Finally, a photovoltaic fiber based on a dye sensitized solar cell technology is demonstrated. This type of fiber acts as a fibrous photo-detector, but the obtained results are poor (short circuit current at nA level). Low performance of the photovoltaic fiber originates from the poor quality of a TiO_2 layer and from the low intensity of light penetrating into the dye sensitized solar cell structure.

Preface

I wish to express my gratitude to my supervisor Professor Ali Harlin for his guidance throughout this work. I especially thank him for giving me the opportunity to work independently. I would also like to thank the head of the Laboratory, Professor Pertti Nousiainen, for his guidance and help with financial issues.

I am indebted to Maritta Suoniemi and Riitta Salonen for dealing with bureaucratic issues related to my studies throughout these five years. My warmest thanks go to my roommate Pirjo Heikkilä, PhD, for proofreading my articles, thesis, and taking SEM pictures included in this thesis. I want to thank all my former colleagues from the Laboratory of Fiber Materials Science for their support, especially in my attempts to study Finnish language.

I would like to thank Minna Toivola for her help in making photovoltaic fibers and for fruitful discussions on the topic of dye sensitized solar cells.

The official examiners of this thesis, Juha Hartikainen, PhD, and Professor Ronald Österbacka, are gratefully acknowledged for useful suggestions and remarks. I also thank Katrina Wendel for carefully proofreading my thesis.

I would like to express my gratitude to Archimedes Foundation from Estonia and CIMO from Finland for the financial support.

I wish to thank my parents and brothers for their support. Finally, I would like to thank my husband Rain, PhD, and my son Rainer for their love, encouragement, and patients throughout the thesis writing process.

— Marju Ferenets

Tampere, 2009

Contents

List of Original Publications

This thesis is based on the following original publications, hereafter referred to by their Roman numerals:

I M. Ferenets, H. Myllymäki, K. Grahn, A. Sipilä, and A. Harlin, Manufacturing Methods For Multi Step Index Plastic Optical Fiber Materials, *Autex Research Journal* 4 (2004) 164–174.

II M. Ferenets and A. Harlin. Chemical in situ Polymerization of Polypyrrole on Poly-(methyl Metacrylate) Substrate, *Thin Solid Films* 515 (2007) 5324–5328.

III M. Ferenets and A. Harlin. Poly(3,4-ethylenedioxythiophene) Based Optical Sensor for Sensing Ammonia Vapors, *Sensors and Actuators, B, Chemical*, Submitted.

IV M. Ferenets and A. Harlin. Electrical versus Optical Sensitivity of Poly(3,4-ethylenedioxy-thiophene) to Ammonia, *IEEE Sensors Journal*, Submitted.

V M. Toivola, M. Ferenets, A. Harlin, and P. Lund. Photovoltaic Fiber, *Thin Solid Films* 517 (2009) 2799–2802.

List of Abbreviations

Abbreviations

APS	Ammonium peroxydisulphate
DMSO	Dimethyl sulfoxide
DNT	2,4-dinitrotoluene
DSSC	Dye sensitized solar cell
EDOT	3,4-ethylenedioxythiophene
EMI	Electromagnetic interference
FET	Field effect transistor
FeTOS	Ferric(III)tosylate, Fe(III)toluene sulfonate
GI	Graded index
ICP	Inherently conductive polymer
IR	Infrared
ITO	Indium tin oxide
LAN	Local area network
LED	Light-emitting diode
MSI	Multi-step index
PANI	Polyaniline
PA	Polyacetylene
PEDOT	Poly(3,4-ethylenedioxythiophene)
PES	Poly(ether sulfone)
PET	Poly(ethyleneterephtalate)
PMMA	Poly(methyl metacrylate)

POF	Plastic optical fiber
ppb	Part per billion
ppm	Part per million
PPV	Poly(*p*-phenylenevinylene)
PPy	Polypyrrole
PSS	Poly(styrene sulfonate)
PTSA	*p*-toluene sulfonic acid
PTS	*p*-toluene sulfonate
RH	Relative humidity
RI	Refractive index
SEM	Scanning electron microscopy
SI	Step index
SOF	Silica optical fiber
TCO	Transparent conducting oxide
TFT	Thin film transistor
TGA	Thermogravimetric analysis
TNT	2,4,6-trinitrotoluene
VPP	Vapor phase polymerization

Symbols

A	Absorbance
η	Power conversion efficiency
eV	Electronvolt
FF	Fill factor
J_{sc}	Short circuit current density
λ	Wavelength
R_S	Surface resistivity
T	Transmittance
V_{oc}	Open circuit voltage

CHAPTER 1

Introduction

The driving forces of optical fiber technology are mainly telecommunication networks as well as local area networks (LAN) and automotive applications, but sensing and lighting are also important application areas of optical fibers. The main advantage of optical fibers compared to traditional copper wires is their higher transmission speed, higher bandwidth (especially for silica optical fibers (SOF)), immunity to electromagnetic interference (EMI), lower transmission losses, and lower weight. Plastic optical fibers (POF) are cheap, easy to assemble, and lightweight. Data transmission properties of POF are limited to less than 100 m connection links being applicable, for example, in campus or domestic networks as well as in devices.

An optical fiber substrate offers an interesting starting point for several device schemes such as being used for lighting inside activating the structure deposited on top of the fiber. For example, fiber lasers are made by adding active components (e.g. laser dye, gain material) to the optical fiber core or cladding. The other group of functional optical fibers comprises fiber-optic sensors. In this case usually either the core or the cladding of the optical fiber is modified by some active material that is sensitive to some analyte. Planar sensing elements are used in combination with optical fibers. Fiber-optic sensors are especially favored due the possibility of remote and distributed sensing. Its electrical part is isolated from the measurement site, hence the fiber-optic sensors are suitable for environments with explosion hazard. The small size of optical fibers enables usage of them for sensing in confined places.

On the other hand there are several new types of electronic and optical materials emerging. Among those are the promising inherently conductive polymers (ICP). ICPs are electrically conductive upon doping, have electrochemically tunable optical properties and are compatible

with polymeric substrates (e.g. poly(ethylene terephtalate) (PET), poly(methyl metacrylate (PMMA) in a sense of low processing temperatures and are flexible.

The discovery of ICPs has lead to a new technology called "organic electronics" (sometimes also referred to as "plastic electronics"), which means electronics based on devices manufactured of organic materials (molecular solids, oligomers, or polymers). The main motivation of organic electronics is the ability to use organic materials in field-effect-transistor (FET) based circuits fabricated on a large area and in flexible substrates [1]. Other electronic and optoelectronic devices made of organic materials include light-emitting diodes (LEDs), electrophoretic display pixels, photovoltaic cells, and physical and chemical sensors. The use of organic electronic materials enables low-cost, high-throughput printable electronic devices. For organic materials desired properties can be tailored quite precisely during synthesis. An especially attractive possibility is the ability to manufacture electronic devices by the roll-to-roll processing method (e.g. printing) as it would enable cost-effective production.

Another advantage that organic and printed electronics has is the ability to form electronic devices (e.g. thin film transistor (TFT)) on highly curved substrates such as fibers [1]. Such device architecture would enable integration of optoelectronic elements into wearable devices like clothing or confining them into limited spaces. This would be rather problematic to realize with traditional inorganic materials although there is extensive on-going research also in making inorganic electronic materials compatible with plastic substrates.

In fabrication of fiber devices one of the crucial points is the compatibility of device materials and their deposition techniques with fiber materials and cylindrical geometry. Suitable deposition methods are, for example, dip coating, painting, and vapor deposition techniques. The latter ones are often limited in a sense that they require vacuum or high processing temperature that makes those techniques expensive and/or incompatible with polymeric fibers. Such techniques are also rather expensive and continuous processing is problematic to achieve.

The aim of this thesis is to study how to combine optical and ICP materials preferentially in the fiber form. This goal has been first realized in studying the practical issues connected with POF manufacturing. The study continued by the *in situ* polymerization of two different ICPs—polypyrrole (PPy) and poly(3,4-ethylenedioxythiophene) (PEDOT)—on PMMA substrate. The use of such thin ICP films were studied as transparent electrodes and chemical

sensing elements. Both of those applications would be compatible with optical fiber devices. Finally, a photovoltaic fiber was built on an optical fiber converting light energy propagating in the optical fiber and partially penetrating into the photovoltaic structure into electrical energy.

Throughout this research the aim has been to find an optimum solution between device simplicity, cost-effectiveness, and performance. There are very sophisticated and precise optical measurement methods available, but those devices are expensive, require well-trained users, and are often bulky and not portable. Also there is a use for simple, straightforward optoelectronic devices, and so this research has concentrated on studying possibilities of accomplishing these devices. According to this principle rather simple processing and measurement techniques have been used in this research.

This thesis consists of three main chapters: Chapter 2—Literature Review, Chapter 3— Materials and Methods, and Chapter 4—Results and Discussion. Chapter 2 gives a short overview of POF and about different kinds of functional optical fibers. The principle of dye sensitized solar cells (DSSC) is introduced. Synthesis and properties of ICPs as well as their use in sensors is also reviewed in Chapter 2. In Chapter 3 experimental details of ICP synthesis and characterization are described. The set-up and sensitivity calculations of PEDOT-based NH_3 sensor are explained in Chapter 3. The preparation details of photovoltaic fibers are also given in this chapter. The most significant results and findings of this thesis are presented and discussed in Chapter 4. It has to be mentioned that optical fiber manufacturing is discussed only briefly in Chapters 2 and 4. This is because the experimental issues are thoroughly discussed in article **I** and the optical fibers used in this work are simple step index fibers.

CHAPTER 2

Literature Review

In this chapter a brief introduction of the working principle, performance determining factors, and manufacturing methods of POF is made. After that some examples of functional optical fibers are presented. An important part of this thesis deals with ICPs and, hence, the synthesis, properties, and applications are reviewed in this chapter. Finally, the working principle of DSSC is introduced.

2.1 Plastic Optical Fibers

An optical fiber is a highly transparent dielectric medium that consists of a core and cladding with refractive indices (RI) of n_{core} and $n_{cladding}$, respectively. Light is guided along the core of the fiber by total internal reflection if n_{core}>$n_{cladding}$. Optical fibers can be made of silica or polymeric materials. According to the RI profile optical fibers are divided into step index (SI), graded index (GI), and multi step index (MSI) fibers.

A typical polymer used for POF manufacturing is PMMA with RI 1.492. Other optical polymers are polycarbonate (PC) ($n = 1.58$) and polystyrene (PS) ($n = 1.59$). In MSI or GI fibers the RI is controlled by choosing suitable monomers either increasing or decreasing the RI. Comonomers increasing the RI are, for example, vinyl phenylacetate ($n = 1.567$), phenyl metacrylate ($n = 1.570$), and bromobenzene ($n = 1.56$). For a lower RI typically fluoropolymers (e.g. tetrafluoropropyl metacrylate) are used.

POF have limited transmission properties compared to SOF due to the higher attenuation of the optical signal. Attenuation in optical fibers is mainly attributed to waveguide dispersion and

material dispersion. Waveguide dispersion depends on the RI profile of the optical fiber and it is the highest for SI optical fibers. The smallest waveguide dispersion is for single-mode fibers that have a very small core diameter and are therefore rather hard to assemble and connect. Waveguide dispersion can be reduced by using a gradual or stepwise change in RI from the center of the optical fiber cross-section towards the edges. Those RI profiles are GI and MSI profiles, respectively.

However, the main limiting factor of optical polymers like PMMA, PC, and PS is material dispersion that originates mainly from molecular vibrations of different chemical bonds present in material. In PMMA, for example, C-H bonds cause pronounced absorbance in the infrared (IR) range that makes them useless in the main data and telecommunication wavelengths of 1300 nm and 1550 nm, respectively. PMMA fibers have attenuation minima at 520 nm, 570 nm, and 650 nm. A typical attenuation for SI PMMA fiber is 150 dB/km at 650 nm. For GI PMMA fibers attenuating around 100 dB/km have been achieved [2]. Perfluorinated (CYTOP®) POF have attenuation about 40 dB/km and a high transmission rate of approximately 10 Gb/s for 100 m [3].

Optical fiber manufacturing typically consists of two separate stages:

1. Preform construction.
2. Fiber drawing.

In the preform construction step a thick rod of optical fiber material (plastic or silica) with determined RI profile is made. The preform can be made by different methods: chemical vapor deposition, interfacial gel polymerization technique [4], centrifuging [5], and photochemical polymerization [2]. In the second step the preform is drawn into a fiber with final dimensions. The crucial process parameters are the drawing speed and cooling in order to avoid crystallization that leads to anisotropic optical properties and birefringence. Monitoring of the fiber diameter and concentricity are also important issues [2, 6].

The fiber drawing from the preform is a batch method, but it would be attractive to manufacture optical fibers by continuous methods like extrusion. In the extrusion technique the core is formed by one extruder and the cladding layer is added on top of that. Conical extruders

that enable multilayer extrusion are especially suitable for MSI-POF manufacturing. Typically, the RI profile is obtained by using raw materials of different RI-s, but the extrusion technique based on the dopant diffusion coextrusion has been demonstrated using PMMA doped with diphenyl sulphide ($n = 1.630$) [7].

POF offer an attractive combination of large fiber diameters (typically up to 1 mm) and hence simple assembly, light weight, robustness, and cost effectiveness. Additionally, POF and SOF both are inert to EMI; they are electrically isolated and can be used for illumination or data transmission in humid or explosive environments [6]. The main applications of POF are in short-distance (less than 100 m) communication networks, for example, in automobiles, airplanes, and fiber-in-the-home applications. Also, illumination and physical [8, 9] as well as chemical [10–14] sensors are interesting application areas of POF.

2.2 Functional Optical Fibers

Optical fibers are usually composed of a simple light transmission medium, but those can also be active functional elements. Functionality can be added to optical fibers in different ways. In fiber lasers, for example, a gain material (rare earth metals like erbium, neodymium, ytterbium, and also organic laser dyes) is typically added into the core material and optically pumped. Microring lasers are optical fiber-based lasers having gain material deposited on top of the fiber [15, 16]. In fiber Bragg gratings functionality is achieved by alternating optical materials of different refractive indices in the fiber core [17, 18]. By modifications of the optical fiber cladding, it is possible to construct sensors or interesting illumination solutions. Ring-mode lasing structures using a modification of poly(*p*-phenylenevinylene) (PPV) have been used to detect trace vapors of explosives 2,4,6-trinitrotoluene (TNT) and 2,4-dinitrotoluene (DNT). Optical pumping causes lasing in a thin film of polymer coated on an optical fiber. Lasing is quenched at the presence of 5 ppb TNT. Such a sensor can be used for detecting explosives, for example, in airports or other public places and also for finding buried landmines [19].

It is also possible to combine optical fibers with metal wires or other non-optical components and obtain both optically and electrically functioning fibers. An integrated self-monitoring optical transport fiber has been developed enabling optical transport via the photonic band-gap

structure and temperature monitoring elements along the entire fiber length. The fiber transmission element use a hollow-core multilayer cylindrical photonic band-gap structure designed to guide 10.6 μm radiation. Temperature detection elements comprise metal wires placed in the vicinity of the hollow core. Metal wires bridged by the semiconductor layer extend along the entire length of the fiber and deliver the electrical response to the fiber ends [20]. A tunable fiber photodetector depicted in Fig. 2.1 has been made comprising an amorphous semiconductor core in contact with metallic nanowires, and surrounded by a cylindrical-shell resonant optical cavity. Such fibers have been arranged in the form of a "spectrometric fabric" that would enable large-area optoelectronic functional surfaces [21]. Semiconductor optoelectronic devices have been built inside the micro-structured optical fibers using high-pressure microfluidic chemical deposition [22]. A fiber-integrated germanium field effect transistor (FET) were demonstrated with SiGe and SiAu heterostructures. Such micro-structured optical-fiber integrated semiconductor/metallic devices would enable electro-optic modulation of the semiconductor RI and also a nonlinear frequency conversion in the near- to mid-IR wavelength range.

An optical fiber based organic photovoltaic device using poly(3-hexylthiophene) and 1-(3-methoxycarbonyl)-propyl-1-phenyl-(6,6)C_{61} (P3HT:PCBM) bulk heterojunction blends as the absorbing material has been fabricated onto a multimode optical fiber [23]. In those fibers optical fibers were coated with indium tin oxide (ITO) by the sol-gel dip method. PEDOT:PSS and P3HT:PCBM were deposited by dip-coating. Lithium fluoride (LiF) and aluminium (Al) electrodes were deposited by thermal evaporation. The fiber diameter varied from 0.6 mm to 1.5 mm. The best performance was achieved in the case of the smallest fiber diameter ($\eta_{external} = 0.6\%$). It was observed that the cell performance was influenced by the angle of the incident light with the optimal angle of 10° [23].

A low-index Fabry-Perot cavity has been constructed in the form of a fiber. Fibers were made of arsenic triselenide (As_2Se_3), a chalcogenide glass, and poly(ether sulfone) (PES) [24]. The idea was to demonstrate that the spectral position of the resonant Fabry-Perot mode can be reversibly tuned by applying axial mechanical stress. Alternating layers of PES and As_2Se_3 formed two mirrors that transmitted only Fabry-Perot resonance modes . A preform was made of a hollow core polymer rod surrounded by six bilayers of PES and As_2Se_3, separated in the middle by an extra polymer layer. The diameter of fibers varied from approximately 100 μm

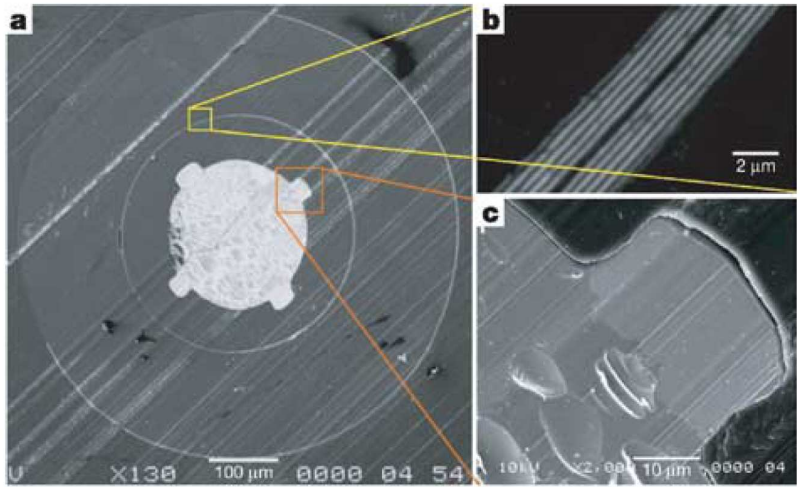

Figure 2.1 — Integrated optoelectronic device fiber. (a) SEM micrograph of the entire cross-section of a 650 mm-thick device fiber with a 200 mm chalcogenide glass core surrounded by a PES cladding. The core region is surrounded by a resonant cavity structure (eight pairs of l/4 As_2Se_3/poly(ether imide) multilayers, with a l/2 resonant cavity in the middle). The bright regions on the polymer-glass interface are the Sn metal electrodes, 18 mm thick and 30 mm wide, which are continuous along the whole fiber length. (b), A magnified micrograph showing the resonant optical cavity structure. (c) A magnified micrograph demonstrating the excellent quality of the semiconductor-metal interface [21].

to approximately 420 μm. The Fabry-Perot mode differed for each fiber diameter [24].

The working principle of the modified cladding fiber-optic sensors is based on the evanescent field of light penetrating into the cladding layer of the optical fiber. Light traveling in an optical waveguide is confined to the high RI core, but light energy associated with bound guided modes also penetrates into the surrounding lower RI cladding medium. The electric field amplitude of the light, E, that is called the evanescent field, decays exponentially with distance x into the optically thinner medium (see Fig. 2.2 (b)):

$$E = E_0 \cdot \exp\left(-\frac{x}{d_p}\right), \tag{2.1}$$

where E_0 is the electric field at the surface of the waveguide. The depth of penetration, d_p, is defined as the distance for the electric field amplitude to fall to 1/e of this value at this surface:

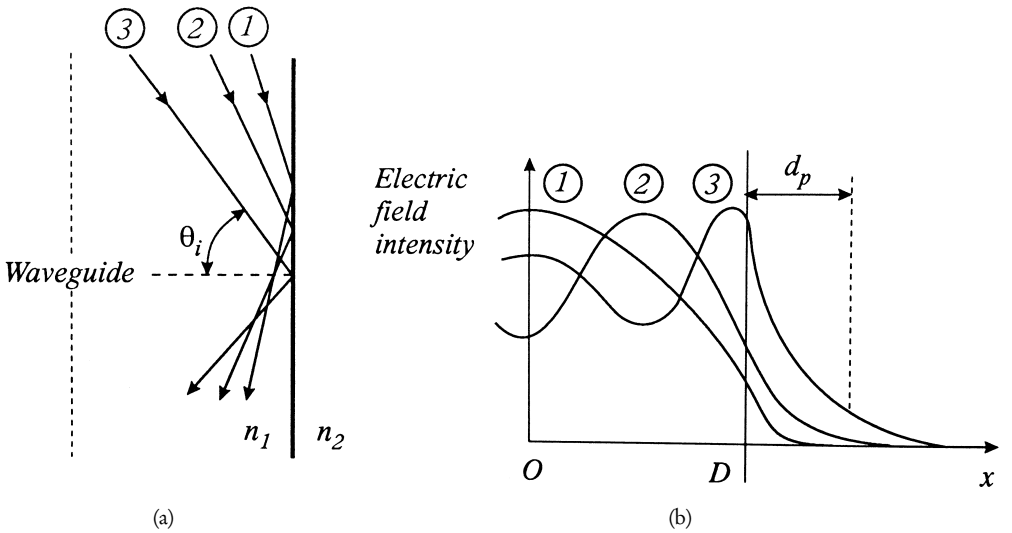

Figure 2.2 — Principle of evanescent field spectroscopy: (a) Light guided inside the waveguide measures the material with RI n_2. Three rays of light are shown with different incident angles. (b) The electric field of the three rays falls exponentially outside the waveguide. The highest order mode, 3, with the highest incidence angle, θ_i, has the largest penetration depth, d_p, into the surrounding medium [26].

$$d_p = \frac{\lambda}{2\pi n_1 \sqrt{\sin^2\theta - \left(\frac{n_1}{n_2}\right)^2}}, \tag{2.2}$$

where n_1 and n_2 are the RIs of the waveguide and the surrounding medium, and θ is the angle of propagation in the guide. Higher order modes (with higher θ) have a larger penetration depth and the intensity of the electric field E_0 at the core cladding interface is higher (see Fig. 2.2). The penetration depths are typically 50 nm to 1000 nm for visible light ($d_p < \lambda$ [25]). The measurement of a chemical reaction by a light traveling inside the waveguide can be realized via scattering by molecules on the surface by absorption or fluorescence changes [26].

Evanescent field spectroscopy or sensing techniques are used for measuring chemical reactions on the surface of a waveguide that can be in the form of a slab guide, a planar integrated-optic guide, or an optical fiber. The waveguide can be coated with a reagent (e.g. dye) that will react with the analyte [26].

2.3 Inherently Conductive Polymers

Inherently conductive polymers were first discovered by Heeger, Shirakawa, and MacDiarmid in 1977 [27]. They observed that if the thin film of a neutral polyacetylene (PA) was treated with iodine vapors its electrical conductivity increased by seven orders of magnitude. The mechanism of electrical conductivity in ICPs is attributed to the π-conjugated molecular structure of those materials. ICPs are semiconducting materials that can either be *p*-type (i.e. hole-conducting) or *n*-type (i.e. electron-conducting). The importance of this discovery was emphasized by the Nobel Prize in 2000.

2.3.1 Synthesis

There are four main synthesis methods of ICPs:

1. Chemical oxidative polymerization in bulk or *in situ*.
2. Electrochemical polymerization.
3. Vapor phase polymerization (VPP) also known as chemical vapor deposition.
4. Plasma polymerization.

Synthesis of ICPs can be divided into two distinctive steps:

1. Formation of the polymer chain.
2. Doping.

The ICP polymerization mechanism is not fully known, but it is widely accepted that in the first step monomer units are oxidized by the oxidant (e.g. ammonium peroxydisulfate (APS), ferric ions, permanganate or bichromate anions, or hydrogen peroxide) to form a radical cation. It has been proposed that the cation radicals form dimers by radical-radical coupling (Fig. 2.3). This chain building process continues via formation of the oligomeric species [28]. Finally, when the chain length increases, solubility of the polymer decreases and a film of polymer is formed on the substrate, or polymer particles are formed and precipitated. During the doping a counter-ion (i.e. the dopant) is inserted for charge balancing. If the reaction time is too long or the oxidant is very strong, overoxidation of ICP may take place. In overoxidation unfavorable

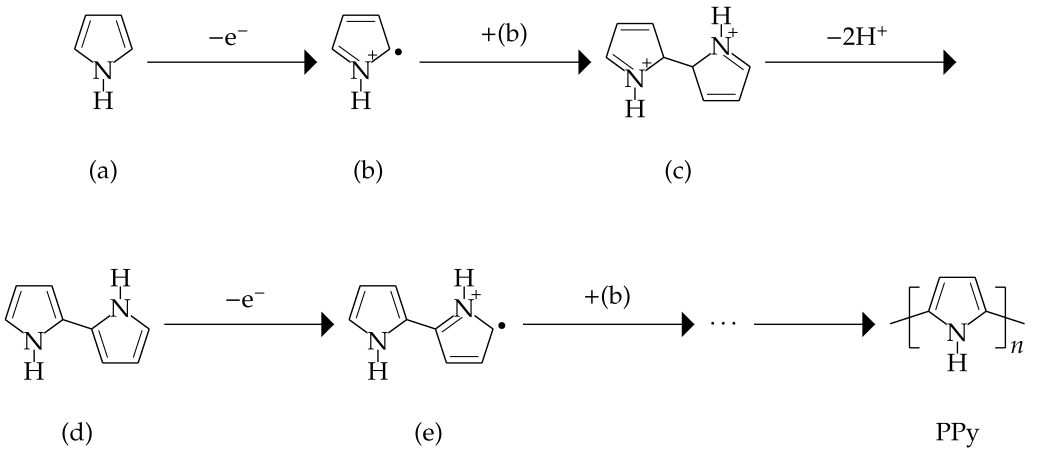

Figure 2.3 — Mechanism of oxidative polymerization of pyrrole [28].

chemical sidegroups are formed leading to the reduced conjugation length, hence lowering the conductivity of the polymer [29–31].

In electrochemical synthesis the polymerization is initiated and doping is carried out by electrochemical oxidation. Electrochemical polymerization of PPy has been demonstrated, for example, in [32, 33]. Characteristic to electrochemical polymerization is that polymer films are obtained directly on the electrode (anode). This leads to the main drawback of this method—the film area (size) is limited to the size of the electrode, and therefore the insulating substrates cannot be coated with ICPs by electrochemical synthesis. The advantages of electrochemical polymerization are easy control of the film thickness and oxidation state of the polymer (oxidized or neutral) [34]. Other characteristic features of electropolymerized ICPs are large porosity [32] and uneven surfaces of the resulting ICP films.

VPP is a polymerization method where the solution of the oxidant is first deposited on to the substrate. This substrate is subsequently exposed to the vapors of a monomer, and polymerization occurs in sites where the oxidant and the monomer come in contact with each other [35]. It is a partly dry method meaning that it is not necessary to put the whole substrate into a wet environment during the film forming process. For instance, this is especially favorable in the manufacturing of multi-layer electronic devices. The VPP technique also enables the

patterning of the ICP thin films at the required place with the required size and shape (e.g. the oxidant solution is printed on the substrate). However, the excess reaction components have to be removed and for that a washing step is needed.

In plasma polymerization the cation radicals necessary for chain formation are induced by the plasma. Doping of the polymer can be carried out simultaneously with polymerization [36] or as a separate step [37, 38]. Plasma polymerized films of PPy have been demonstrated to be very smooth and uniform [38], but the resulting polymer has a rather amorphous structure. The plasma cleaves the monomer (e.g. pyrrole) rings, which causes the side reactions resulting in branching and cross-linking that leads to a decreased conjugation length. For that reason plasma polymerized films tend to have a very low conductivity (e.g. $4.8{\cdot}10^{-8}$ S/cm). It has been observed that in the case of PPy, plasma polymerized PPy is environmentally more unstable compared to chemically polymerized PPy. The reason for that is the instability of the charge transfer complex formed from $-N^+$-species in the plasma polymerized PPy [38].

The nature of the counter-ion significantly influences the properties of the ICPs. For example, the use of larger counter-ion molecules have been used to enhance the processability of ICPs. Usually smaller counter-ion molecules lead to a more closely packed crystalline structure and hence to a higher electrical conductivity [31, 34].

2.3.2 Electrical and Optical Properties of ICPs

The charge transport in ICPs is proposed to take place along the conjugated chains (intrachain transport) with interchain hopping as a necessary secondary step [39, 40]. The intrachain mobility is restricted by conformational and chemical defects (side groups and end groups) in the ICP molecular backbone formed during synthesis [31]. The defects break the conjugation length and reduce the π-orbital overlaps. The charge carrier transport mechanism in the ICPs of granular conformation (e.g. PEDOT:PSS and PPy doped with camphor sulfonic acid or *p*-toluene sulfonic acid) can be explained by the charging energy limited tunneling model, originally proposed for highly disordered conducting polymers. According to this model conduction is supposed to proceed from tunneling between small conducting grains separated by the insulating barriers [41–43]. In this model the conducting clusters are described as highly

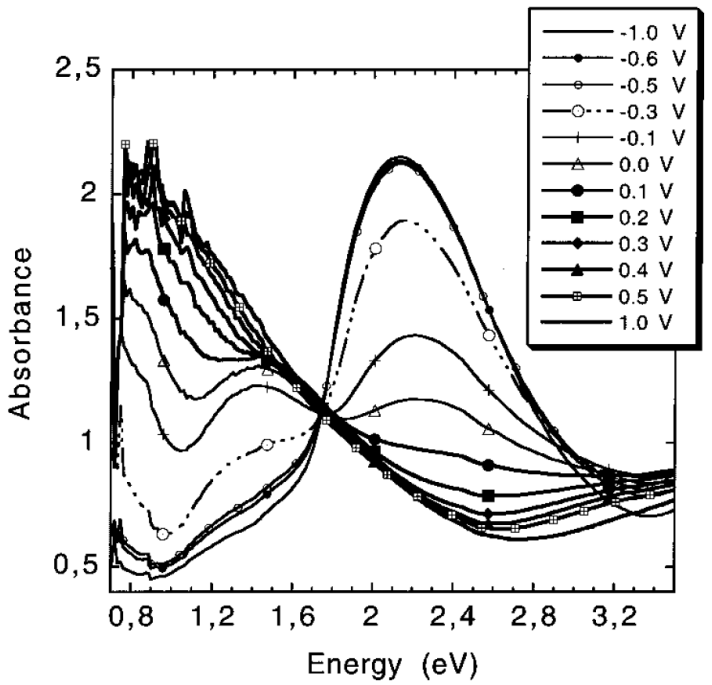

Figure 2.4 — Optical properties of electropolymerized PEDOT [45].

doped "polaronic islands" generated by heterogeneities in the doping distribution. The dopant centers act as bridges between the neighboring chains and therefore improve the charge carrier transport.

Electrical and optical properties of ICPs depend on the doping level of the material. This dependence of optical properties of PEDOT is depiced in Fig. 2.4. In neutral PEDOT (i.e. at potential −1.0 V) $\pi-\pi^*$ absorption is dominant [44]. At a polymerization potential of −0.3 V, the subgap absorption appears at 1.3 eV, 1.5 eV, and 0.75 eV, and when the band gap absorption decreases, the polymer is probably in the polaron state. At a polymerization potential of 0.2 V, the band gap absorption has disappeared, and the subgap absorptions of 1.3 eV and 1.5 eV merge into one absorption band at around 1.5 eV, which is thought to be bipolaronic. At a polymerization potential of 0.5 V, the absorption peak at 1.5 eV has disappeared, and the polymer is in the heavily doped metallic state [45].

2.3.3 Polypyrrole

PPy is a *p*-type semiconducting polymer that has proven to be relatively highly conductive, easy to synthesize, and environmentally stable. PPy can be prepared by chemical [33, 38, 46], electrochemical [32, 33], plasma [37, 47], and vapor phase [35, 48] polymerization. In applications like coating dielectric materials, the most suitable process is the *in situ* chemical polymerization because it provides a relatively high conductivity as well as a suitable thickness and uniformity of the thin film.

The nature of the counter-ion (i.e. the dopant) has greatly influences several properties like conductivity, morphology, and solubility of ICP. Small counter-ions like Cl^- result in a tightly packed fibrillar molecular structure due to the strong inter- and intramolecular interactions and are insoluble. Surfactants like sodium dodecylbenzenesulfonate, sodium alkylnaphthalenesulfonate and sodium alkylsulfonate enhance the conductivity, increase the polymerization yield and also improve the thermal and moisture stabilities in air at 125 °C and at 85 °C and 85% RH [49]. Various types of sulfonic acid dopants have been used for the synthesis of soluble PPy and other ICPs [43]. PPy doped with dodecylbenzene sulfonic acid and different naphtalene sulfonic acids (NSAs) were soluble in *m*-cresol. β-naphtalene sulfonic acid had fibrillar morphology and the highest conductivity (18 S/cm). Other sulfonic acid dopants had a granular morphology and a lower conductivity.

The combination of PMMA and PPy has been studied earlier in the form of composite materials mainly in order to overcome the poor mechanical properties of pure PPy films. The first attempt was made in 1988 when PPy-PMMA composite films were prepared by the chemical polymerization route by spreading the water-insoluble solvent solution of pyrrole and the PMMA mixture on the surface of the aqueous solution containing $K_2S_2O_8$ as the oxidizing agent [50]. The PPY/PMMA bulk composite materials and PPy-coated PMMA particles have been prepared in an aqueous dispersion medium by chemical polymerization. Depending on the PPy content (0.25–10 wt%), the conductivity levels of compression molded samples varied between 10^{-9} S/cm and 0.1 S/cm [51]. The PPy/PMMA core/shell nanospheres have been prepared in order to achieve better dispersion of PPy nanoparticles in a matrix polymer. About 20 μm thick films prepared by compression molding demonstrated an electrical conductivity

in the range of 10^{-1} S/cm to 10^{0} S/cm and 83% transmittance in the visible-light region [52].

PPy has also been used for the preparation of conductive elastomeric blends [53]. In the field of organic electronics, PPy has been studied for the hole-transport layer in polymer LEDs [54] and photovoltaic cells [55] and for the semitransparent bilayer electrode [31, 32]. Other possible applications of PPy are gas [56, 57] and strain sensors [58]. PPy has also been used in combination with textile fibers for EMI shielding fabrics [59]. PPy coated textiles have been studied in [46, 60]. In addition, PPy filled polypropylene fibers have been made [61]. Polyester and polyamide-based conductive fibers have been demonstrated in [62].

2.3.4 Poly(3,4-ethylenedioxythiophene)

Among other polythiophenes PEDOT is one of the most studied polymers due to its excellent electrical conductivity (up to 550 S/cm in the electrochemically doped state), electrochromic properties, and high stability [63]. The better conductivity and environmental stability of PEDOT compared to, for example, PPy [64] can be attributed to its chemical structure. The formation of irregularities such as the α—β bonds and the β—β bonds is prevented because the β and β positions of a thiophene ring are blocked by an ethylenedioxy group [65].

PEDOT has an electronic band gap, defined as the onset of the $\pi - \pi^*$ absorption of 1.6–1.7 eV and a λ_{max} of approximately 610 nm, making it deep blue in color [66]. The low band-gap (i.e. 0.5 eV lower than that of PT) of PEDOT leads to very pronounced electrochromic properties since the doped polymer is almost transparent with a sky-blue tint, and the neutral polymer is blackish-blue. The low band-gap also enables the *n*-doping by electrochemical methods [67]. Electrochemical switching has been carried out for chemically deposited PEDOT films even on the insulating substrate as PET films [68].

The most common *in situ* polymerization method of PEDOT is the base inhibited polymerization first reported by de Leeuw [69]. In this technique imidazole is used to control the polymerization speed of EDOT using the ferric(III)tosylate (FeTOS) oxidant. Imidazole acted as a base, inhibiting the activity of Fe(III). A base inhibitor reduces the oxidation strength of the oxidant. A too active oxidant can cause unwanted bond cleavage in the monomer leading to structural defects in the polymer that disrupt conjugation and reduce conductivity [70]. One

problematic feature, however, in that reaction scheme was that the polymerization of such coatings did not start before removing imidazole at 105 °C, whereas it is often favorable to carry out the coating at RT. Another drawback of imidazole—and most other N – H containing chemicals—is that it binds as ligands to Fe(III) that causes crystallization in the solution leading to the uneven film formation [71]. Other base inhibitors such as pyridine [71, 72] and quinoline [71] have been used in the PEDOT polymerization. Quinoline, however, also needed a thermal treatment to initiate the polymerization process, but no crystal formation was observed. Addition of the pyridine inhibitor increased the pot-life of the oxidant solution and demonstrated also good film forming properties [71]. The reported conductivity of such films was higher than 1000 S/cm.

PEDOT has been chemically polymerized in aqueous solutions using $FeCl_3$ oxidant [73]. The maximum conductivity achieved was 4.3 S/cm. The polymerization of PEDOT in an aqueous medium is problematic due to the insolubility of the EDOT monomer in water. This problem can, however, be overcome by using an emulsion polymerization with an anionic surfactant [65, 74]. The initial problems with moisture stability of such PEDOT were overcome by using *p*-nitrophenol additive [65].

The influence of a solvent used in polymerization mixtures on electrical conductivity of PEDOT doped with FeTOS has been studied in [75]. The highest electrical conductivity was achieved in the case of methanol (20.1 S/cm) and ethanol (9.9 S/cm), whereas the conductivities of PEDOT-acetone and PEDOT-methyl ethyl ketone were as low as $7.6 \cdot 10^{-7}$ S/cm and $2.2 \cdot 10^{-8}$ S/cm, respectively. The enhanced conductivity could be assigned to structural and chemical changes taking place during polymerization. A further investigation of X-ray diffraction patterns of different PEDOT showed that ketone samples were amorphous, and PEDOT made in *n*-butanol and alcohol was crystalline [75].

VPP of PEDOT has been demonstrated in [70–72]. In [70, 71] the mixture of FeTOS (40% solution in butanol) and pyridine was first deposited onto the PET sheets and dried. Subsequently those films were exposed to EDOT vapors in a closed polymerization vessel in either an air, nitrogen or argon environment. The bulk conductivity of these films was approximately 1000 S/cm. In [72] all the reaction components were inserted into the polymerization vessel in a vapor form. The reaction time was 30 min. The best conductivity was 105 S/cm at a

polymerization temperature of 85 °C .

The most common form of PEDOT is commercially available from H. C. Starck under the name of Clevios^{TM} P (formerly Baytron P). Their synthesis was originally developed by Bayer AG [76]. In this reaction the EDOT monomer is polymerized in an aqueous polyelectrolyte (usually PSS) using an $Na_2S_2O_8$ oxidant. The reaction is carried out at RT and gives a dark blue aqueous dispersion of PEDOT:PSS that is easily processable into antistatic coatings and transparent electrodes. Although PEDOT:PSS is available in a form of an aqueous dispersion, films of PEDOT:PSS are highly conductive, transparent, mechanically durable, and insoluble in any common solvent after drying. Aqueous dispersions of PEDOT:PSS can be easily formed into coatings by spin-coating, dip-coating, spraying, ink-jet or screen printing [77].

The structural characterization of insoluble ICPs is rather problematic as the standard solution characterization techniques cannot be utilized [77]. The structural analysis of ICPs can be done, however, in a form of thin films that was demonstrated in [78]. Results of an X-ray diffraction analysis showed that PEDOT doped with FeTOS is very anisotropic with a limited crystalline structure in those films. Dopant molecules form planes between the stacks of polymer chains parallel to the substrate. It was also found out that heating the material to 200 °C caused an increase in crystallinity that had not been observed for other substituted polythiophenes. The optical properties of PEDOT have been demonstrated to also be anisotropic and of uniaxial character with the optical axis normal to the film surface [63, 79]. The same anisotropy of optical properties was observed in spin-coated PEDOT:PSS films [80]. The anisotropy was decreased and conductivity was increased by adding sorbitol to the PEDOT:PSS dispersion. It has been proposed that sorbitol acts as a plasticizer in PEDOT:PSS, thus decreasing the inter-chain interactions and enabling better reorientation of polymer chains. During heating in sorbitol-containing films, PEDOT:PSS chains may reorient with a more favorable inter-chain interaction between PEDOT units. On the other hand the activation energy decreases for a charge transfer, thus increasing the conductivity [80]. The temperature dependence of the electrical conductivity of PEDOT:PSS has been found to be characteristic of strongly disordered structures (e.g. similar to granular metals) [42].

PEDOT is already used, and its potential usages have been studied for several more applications. PEDOT:PSS has been used for antistatic coatings [77, 81]. PEDOT has been used as

a replacement for a liquid electrolyte in dye sensitized solar cells [82] and also for large area semi-transparent electrodes of photovoltaic applications [83]. PEDOT has been polymerized *in situ* on various substrates (e.g. on synthetic fibers [84, 85]). A transparent electrically conductive glue was developed on the basis of PEDOT:PSS with D-sorbitol that acts as an adhesive component. A polymer LED using PEDOT:PSS (D-sorbitol) buffer layer was demonstrated in [86]. Transparent and flexible all-organic FETs were made using PEDOT and PPy in conductive layers and poly(vinyl cinnamate) or epoxy/methacrylate in the insulating layer [87]. FET using PEDOT:PSS electrodes has also been made in [88].

2.3.5 ICPs in Sensor Applications

As mentioned earlier ICPs such as PPy, polyaniline (PANI), and polythiophene (PT) show interesting chemical and physical properties derived from their unique conjugated π-electron system. The oxidation level of conducting polymers is easily affected by chemical or electrochemical doping/dedoping (oxidation/reduction) mechanisms, causing a sensitive and rapid response to specific chemical species. These features allow conducting polymers to be utilized as versatile optical and electrical sensors [52]. The electrical sensors have been more widely studied, but quite a number of optical ICP sensors has also been demonstrated.

Optical gas sensors based on ICP have been demonstrated in measuring different kinds of chemical species. A chemical sensing technique for detecting the nerve agent dimethylmethylphosphonate (DMMP) has been presented in [56]. This technique used a combination of doped PPy as an active chemical material coated on an optical fiber to form an intrinsic fiber-optic sensor. The sensitivity of up to 26 ppm of DMMP with a response time of a few seconds was demonstrated. Two processing techniques of PPy—*in situ* deposition and VPP—were compared. The scanning electron microscopy (SEM) characterization study revealed that the polymer deposited by *in situ* deposition had a nonuniform but highly porous coating, which gives a highly sensitive but a weakly adhesive coating. The VPP on the other hand gives a strongly adhesive but a less sensitive coating due to less porosity and small pore size.

The optical sensitivity of PANI to ozone has been studied in [89]. Poly(2-chloroaniline), poly(N-methylaniline) and PANI films were prepared by chemical oxidative polymerization

followed by treatment with the reducing agent disodium disulfite. The resulting films showed significant wavelength dependence of the ozone-sensitive absorbance changes in the visible/near-IR wavelength region at RT. The optical absorbance of the poly(2-chloroaniline) film was sensitive to concentrations as low as 2.5 ppm ozone in air but showed saturation of sensitivity to ozone at concentrations higher than 50 ppm. By contrast, the poly(N-methylaniline) and PANI films did not show a detectable sensitivity to ozone at concentrations of 2.5–10 ppm. However, the high sensitivity of 50–100 ppm ozone was displayed without any saturation. The absorbance change of the polymer films on exposure to ozone was fast, but the slow and incomplete recovery observed on removal of ozone is not favorable for purposes of continuous sensing. The PANI-based optical sensors have been used for detecting ammonia. The planar films of PANI had a response time of less than 15 s and a regeneration time of less than 2 min at RT. The sensors had a detection limit of 1 ppm (v/v) for ammonia with a linear dynamic range from 180 ppm to 18000 ppm [90]. The chemically-deposited PANI films were used for detecting gaseous nitrogen dioxide by an optical method [91]. NO_2-induced optical transmittance changes of the PANI films varied between 5% and 80% for NO_2 concentration of 3–50 ppm.

An amperometric ammonia sensor based on PPy was demonstrated for measuring NH_3 of micromolar concentrations [92]. An electrical gas sensor for ammonia based on the *in situ* polymerized PANI on polyamide 6 fabric has been reported [93]. The influence of different redoping agents was studied on ammonia sensitivity. The PANI-polyamide 6 composite fabrics redoped with formic acid, acrylic acid, and trichloretic acid demonstrated sensitivity from 50% to over 300% and with a response time of 5 min.

The remote sensing of ammonia has been demonstrated at a wavelength of 1300 nm with PANI films over 100 m using standard telecommunication technology [94]. PANI sensing films were found to respond to ammonia concentrations down to 6 ppm at 50% RH, while being insensitive to the humidity variations in the range of 30–70% RH. The reproducible results were obtained with PANI films older than 2 years.

PEDOT:PSS in a form of printing ink has been used for the detection of organic vapors (alcohols) [95]. PEDOT:PSS thin films exhibited a change in their resistivity in exposure to methanol. PEDOT has also been used to detect morphine [96]. PEDOT doped with perchlorate ions was electrochemically deposited on carbon fibers, pencil leads and glassy carbon

electrodes and used as a solid state sensor for different anions [97]. The best selectivity coefficients were achieved for SCN^-, CO_3^{2-}, and I^-. Spin coated films of PEDOT:PSS were used as an electrical microsensor for soil moisture measurements [98]. The change in the output resistance of the sensor device was observed to be from 2.5 MΩ to 4.0 MΩ, when exposed to soil samples with a gravimetric water content in the range of 15% to 35%.

2.4 Dye Sensitized Solar Cells

In a DSSC light is absorbed by a sensitizer, which is anchored to the surface of a wide-band semiconductor (Fig. 2.5). The charge separation takes place at the interface via photo-induced electron injection from the dye into the conduction band of the solid. The carriers are transported in the conduction band of the semiconductor to the charge collector. A wide band-gap semiconductor (mostly TiO_2, band-gap energy $E_g = 3 - 3.2$ eV) is in the form of nanometer-sized particles which have been sintered together to ensure electrical conduction. A monolayer of charge transfer dye is attached to the surface of the nanocrystalline film. The photo excitation of the dye injects an electron into the conduction band of the oxide. The original state of the dye is subsequently restored by the electron donation from the electrolyte. The latter is usually an organic solvent containing a redox system such as the iodide/triiodide couple. The regeneration of the sensitizer by iodine prevents the conduction band electron from being recaptured by the oxidized dye. The regeneration of the iodide takes place by the reduction of triiodide at the counter electrode and the circuit being completed via electron migration through the external load. Thus the device generates electric power from light without suffering any permanent chemical transformation [99]. Typical elements of a DSSC are a TCO electrode, mesoporous TiO_2, dye, electrolyte, and a counter electrode.

At the beginning of DSSC development, liquid electrolytes were used; however, it is rather problematic to deposit liquid electrolyte in a fully automated manufacturing process. It also requires careful sealing, and its long term stability in a harsh environment is not yet known. For that reason in [100] the use of a gel electrolyte, a solid-state electrolyte or a p-conducting polymer material have been studied. The use of PPy as a solid state electrolyte has been demonstrated in [55]. The efficiency of nearly 1% was reported for aged and redoped cells. Typical

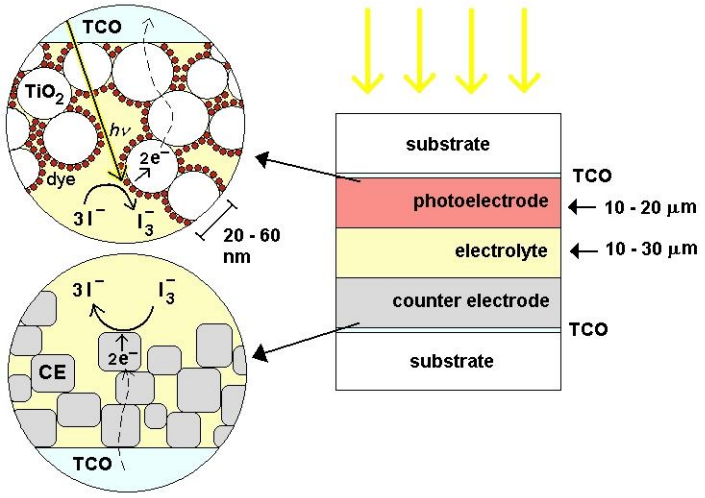

Figure 2.5 — Operation principle of the DSSC from article **V**.

counter electrodes used in DSSCs have been using platinum (Pt) as a catalyst for reduction of triiodide [101]. Pt however is a noble metal, and due to its high price, it is favorable to find a more cost effective counter electrode material.

A DSSC is less sensitive to contamination or the use of impure materials during the manufacturing process than other solar cell types. This enables one to manufacture DSSC without using a clean room environment, while still achieving an efficiency of 7–11% [100].

CHAPTER 3

Materials and Methods

The research reported in this thesis includes a considerable amount of experimental work including optical fiber forming, polymer synthesis and characterization, as well as device design. The details of this experimental work are now discussed in more detail. One exception is made on the MSI optical fiber manufacturing as the experimental details of this work are thoroughly described in article **I**.

3.1 Inherently Conductive Polymers

The practical work made on ICPs included *in situ* chemical oxidative polymerization of PPy and PEDOT in a form of thin films on PMMA sheets or PMMA optical fibers. Typically, the surface resistivity and optical transmittance properties of these films were measured. The surface morphology observations were made with a SEM. The synthesis procedure and conducted measurements are more precisely explained in the following sections.

3.1.1 Polypyrrole

In the case of PPy synthesis, two different polymerization paths were compared using different oxidant/dopant systems. Path I used $FeCl_3$ as an oxidant and dopant. The resulting polymer will be referred to as PPy:Cl. The oxidant/monomer ratio was 2.1. Path II used APS as an oxidant and PTSA as a dopant. Resulting polymer will be referred to as PPy:PTS. Oxidant/monomer ratio was 3.3. The polymerization was carried out in aqueous solutions, the reaction is depicted in Fig. 2.3.

Coating of the PMMA samples took place in a polymerization solution, where samples were kept for a certain period of time. The polymer precipitated or was adsorbed on the sample. Dip-coating of polymerization solution was also tested but was unsuccessful due to the wetting problems. The polymerization solution formed an uneven layer on the PMMA surface due to a high surface energy of water and low surface energy of PMMA.

3.1.2 Poly(3,4-ethylenedioxythiophene)

The PEDOT synthesis was carried out at the surface of a substrate. The polymerization solution consisting of an EDOT monomer, FeTOS oxidant/dopant, pyridine inhibitor and ethanol were mixed and dip-coated or drop-coated on to the substrate. The polymerization solution formed even layer on the PMMA sheets or the optical fibers. The polymerization reaction is depicted in Fig. 3.1. The polymerization occurred at RT during 5–7 min of time. The polymerization was terminated by washing away the unreacted components.

Commercially available PEDOT:PSS Clevios^{TM} PH500 was bought from H. C. Starck. The final mixture contained 5% dimethyl sulfoxide (DMSO) as a conductivity-enhancing solvent suggested in [76]. PH500 is an aqueous dispersion of PEDOT:PSS particles, and hence its inherent wetting properties are rather poor on hydrophobic PMMA. For that reason antifoaming surfactant Surfynol 2502 (Air Products) was added to the coating mixture. The films were deposited by drop-coating.

3.1.3 Electrical Measurements

The electrical properties of ICPs used in this thesis (results presented in articles **II** and **IV**) are characterized in terms of surface resistivity. The surface resistivity is the resistance in Ohms between the opposite edges of a square of the material along the surface of the material [102]. This means that the thickness of the material is not taken into account. It is independent of the electrode dimensions [103]. The surface resistance is the resistance in ohms as detected by using specified electrodes placed on the surface of the material.

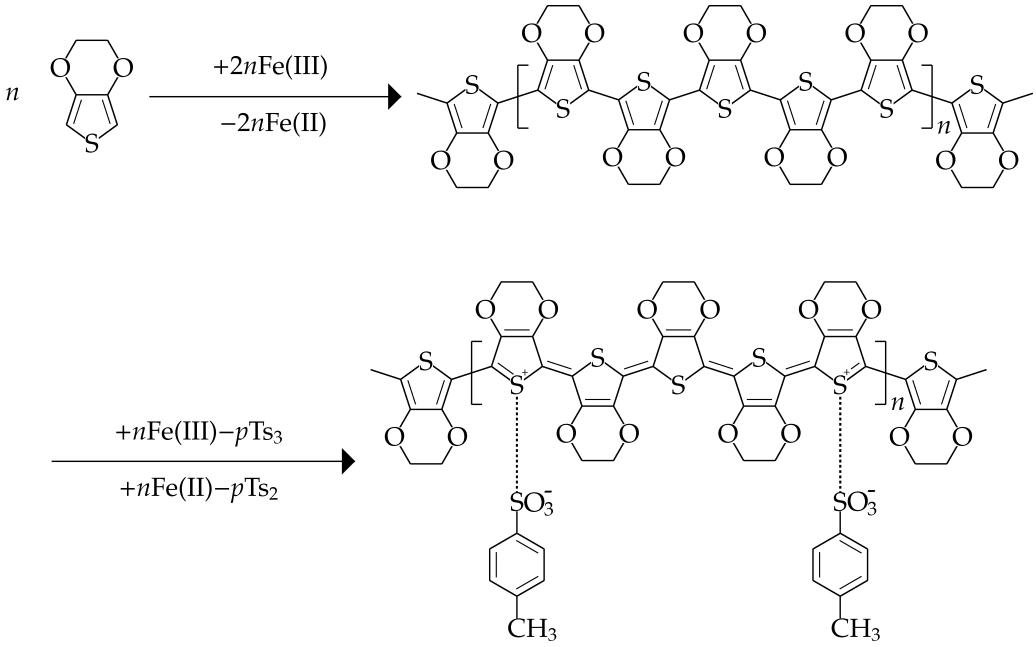

Figure 3.1 — Polymerization reaction of PEDOT:PTS [81]

The surface resistivity was first introduced in [104]. It was stated that a thin film resistor is directly proportional to the resistivity, ρ, and inversely proportional to the thickness, d. The surface resistivity, R_S was defined as follows:

$$R_S = \frac{\rho}{d}. \tag{3.1}$$

A thin film resistor consisting of a simple rectangle of length L and the width W has a resistance of

$$R = \frac{\rho}{d} \cdot \frac{L}{W} = R_S \cdot \frac{L}{W}. \tag{3.2}$$

The term $\frac{L}{W}$ is sometimes referred to as the number of squares in the resistor, since it is equal to the number of squares of side W that can be superimposed on the resistor without overlapping. The term “squares” is dimensionless.

An electrical surface resistance was measured by the 2-probe method [105] using a multimeter, Megger BM80/2. The surface resistivity, R_S, was calculated by the following equation:

$$R_S = R \cdot \frac{W}{L}, \tag{3.3}$$

where R_S is the surface resistivity in units [Ω/sq], R is the measured surface resistance by the 2-probe method, L is the distance between the electrodes (7 mm), and W is the width of the electrodes (6 mm).

3.1.4 Optical Measurements

Ultraviolet-visible (UV-Vis) spectrophotometry was used for determining the optical properties of ICP films.

The absorbance of a material is expressed as:

$$A = \log_{10}\left(\frac{I_0}{I}\right), \tag{3.4}$$

where I_0 is the intensity of the incident light and I is the intensity of the transmitted light.

Another term used in this thesis for optical properties is transmittance, T, which is defined as follows:

$$T = \frac{I}{I_0} \cdot 100. \tag{3.5}$$

Transmittance is reported as a percentage [%].

The spectrophotometers used in this research where Shimadzu UV-2501PC and Shimadzu UV-160A.

3.2 Sensing Schemes for Measuring Gaseous Ammonia

In gaseous ammonia the sensing described in article **III** of ammonia vapor originated from the aqueous solution of NH_4OH . The concentration of NH_4OH solutions were chosen with

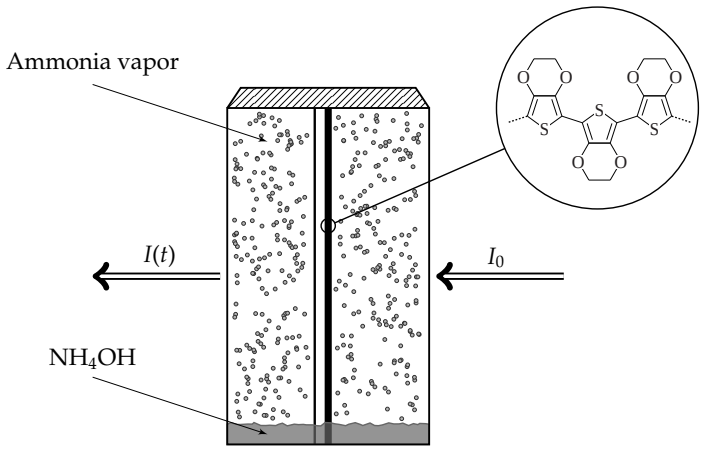

Figure 3.2 — Optical measurement set-up of ammonia sensing.

the following concentrations: 10 mM, 20 mM, 40 mM, 70 mM, and 100 mM. Such solutions will give the following NH_3 concentrations above the solutions: 135 ppm, 274 ppm, 550 ppm, 960 ppm, and 1350 pmm, respectively.

A drop of NH_4OH solution (0.5 ml) was put into the bottom of the cuvette, closed with a lid and let stabilize for 1 min. After that the PEDOT sample was put into the cuvette, and subsequently the changes in optical transmittance were registered. The experimental set-up of ammonia exposure is depicted in Fig. 3.2.

In the comparative study of two different PEDOTs and their optical and electrical responses, the PEDOT samples were thoroughly rinsed with a NH_4OH solution. These results are presented in paper **IV**.

The electrical sensitivity, $S_{electrical}$, was calculated according to the following equation:

$$S_{electrical} = \frac{R_0 - R_S}{R_0} \cdot 100, \tag{3.6}$$

where R_S is the surface resistivity of the NH_3 treated sample and R_0 is the surface resistivity of the untreated PEDOT sample. $S_{electrical}$ is reported as a percentage [%].

The optical sensitivity, $S_{optical}$, was calculated according to the same principle as the electrical sensitivity:

$$S_{optical} = \frac{T_0 - T}{T_0} \cdot 100, \quad [\%], \tag{3.7}$$

where T is the optical transmittance of the NH_3 treated sample and T_0 is the transmittance of untreated PEDOT sample. $S_{optical}$ is reported as a percentage [%].

3.3 Photovoltaic Fiber

The composition of a photovoltaic fiber is depicted in Fig. 3.3. In the case of a PMMA fiber, a photoelectrode was made of 130 nm thick layer of ZnO:Al and 50 nm of TiO_2 deposited by the atomic layer deposition (ALD) method. The sintering step of TiO_2 could not be carried out as PMMA cannot withstand the required temperature (450–500 °C). In the case of glass fibers, the ZnO:Al electrode layer (130 nm) was deposited by the ALD method. TiO_2 was in the form of a paste, and it was deposited by dip-coating. At first the layer was dried at RT for about 10 min and was then sintered at 475–500 °C for 30 min. The quality of the resulting films was not very good, because the subsequential washing with ethanol caused the film to peel off to some extent.

Subsequently, fibers were sensitized in a 0.32 mM solution of a N-719 (cis-bis(isothio- cyanato)bis(2,2'-bipyridyl-4,4'-dicarboxylato)-ruthenium(II) bis-tetrabutylammonium) dye in ethanol for 48 h. Excess dye was rinsed off with ethanol and samples were air dried before applying the electrolyte.

The electrolyte was a gelatinized iodine electrolyte that was heated in order to make it sufficiently liquid for dip-coating. The counter electrode contained graphite powder and carbon black as conductive element, 3-methoxypropionitrile as a solvent, and polyvinylidenefluoride-hexafluoropropylene as a gelatizing agent. A hot (temperature approximately 80 °C) counter electrode mixture was applied by dip-coating on to the solidified electrolyte layer and dried at RT. The resulting counter electrode was a black layer with good mechanical properties.

Photovoltaic fibers were characterized as typical photovoltaic cells by measuring their J–V-curves (Fig. 3.4). The key values obtained from the J–V-curves are the open circuit voltage, V_{oc}, and the short circuit current density, J_{sc}.

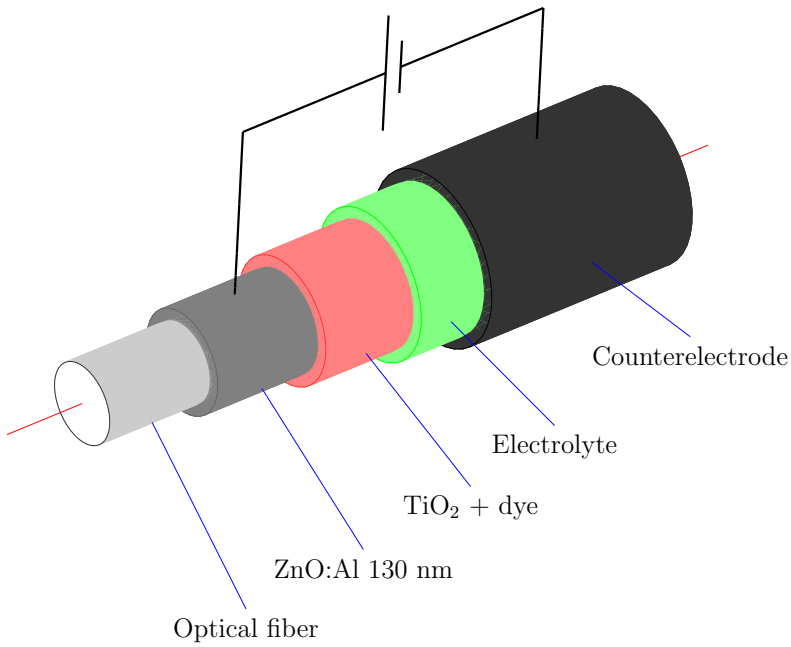

Figure 3.3 — A schematic drawing of the photovoltaic fiber.

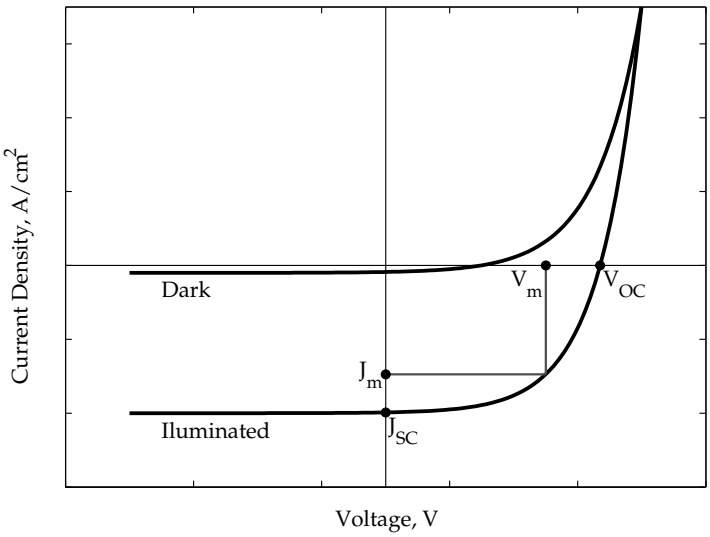

Figure 3.4 — Typical current density vs. voltage (J-V) curves of photovoltaic cells in the dark and under illumination [106].

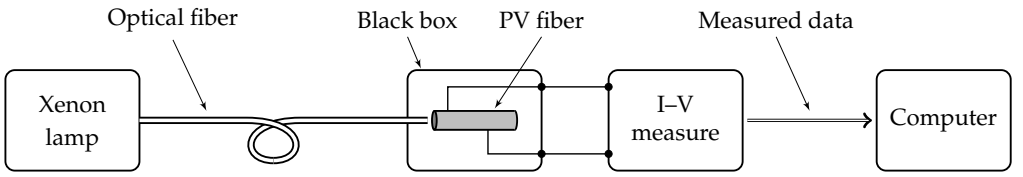

Figure 3.5 — A schematic drawing of the I-V-curve measurements of the photovoltaic fiber.

The operating range of the solar cell is $0 < V < V_{oc}$, where the device generates power. The fill factor (FF) is calculated as follows:

$$FF = \frac{J_m V_m}{J_{sc} V_{oc}}, \tag{3.8}$$

where the product $J_m V_m$ corresponds to the maximum power point.

The power conversion efficiency, η, is calculated as follows:

$$\eta = \frac{J_m V_m}{P_0} = \frac{J_{sc} V_{oc} FF}{P_0}, \tag{3.9}$$

where P_0 is the incident light power.

The set-up of the PV fiber measurement can be seen in Fig. 3.5. A Xe-lamp (Newport, model 6247, 75 W XeHS) was used as a light source. The PV fiber was put into a black box and the electrodes were connected to the I–V-measurement device. A multi-mode optical fiber cable was used to direct the light into the PV fiber.

CHAPTER 4

Results and Discussion

This chapter summarizes the most significant findings made in each area of research discussed in this thesis.

4.1 Multi Step Index Optical Fiber Manufacturing

Optical fiber preform manufacturing turned out to be problematic for various reasons. Clean raw materials and production the environment are important in order to get a high quality preform and hence a good quality optical fiber. Despite monomer purification an extensive formation of bubbles was observed in preforms prepared by thermal bulk polymerization at different conditions. The problem was overcome by using a pressurized polymerization reactor. In that way the low molecular weight residuals of the polymerization process were removed, and the bubbling effect was minimized. Another positive effect of elevated pressure is the reduction of mold shrinkage. Satisfactory results were achieved at a reactor pressure of 25 bar.

A MSI preform formation was not successful by means of the centrifugal force with assisted liquid addition. The chemical vapor deposition technique should have been used instead because it ensures more even deposition of monomers.

Another way for MSI fiber manufacturing used the single screw and conical extrusion techniques. The conical extruder is especially suitable for manufacturing multi-layered products, typically up to six layers simultaneously. Pellets of PMMA and PC were dried before extrusion to remove the humidity. We observed some bubble formation and some impurities in the PMMA fibers. In PC fibers a trace line originating most probably from the nozzle was seen in

polarization microscopy pictures. Some contamination of the PC fiber surface was observed. In this case pellets were used as a raw material. Pellets have an extensive surface area and are therefore easily polluted.

Conical extrusion made fibers of higher tenacity than single screw extrusion. On the other hand, those fibers had more impurities on the surface and inside the fiber. Another drawback was the deformed cross-section of the fiber that was caused by winding up not fully solidified fiber.

The two-layered extrusion set-up consisted of a combination of a single screw and the conical extruders that were connected with a special joint. The core layer made of PMMA was produced by a single-screw extruder and a cladding layer made of PC formed by conical extrusion. Consequently, the concentricity of the core and cladding layers of the resulting fiber was not satisfactory due to the placement of nozzles of the core and cladding materials.

It is rather difficult to obtain a high quality optical fiber with the final dimensions in one formation step. This requires that a thicker preform fiber should be extruded in the first step, which would be drawn to final dimensions in the subsequent production step. Another aspect is the purity of materials and the machinery. It would be favorable to connect the extruder to the polymerization reactor in order to avoid contamination. The cooling distance of the fiber should be increased to avoid the cross-sectional deformation.

The fiber drawing using IR ovens was performed on commercially available preforms. During heating extensive bubbling on the surface and the outer part of the cross-section was observed. The fiber drawing was successful despite bubbling, however, the cross-section of those fibers was not circular. In order to reduce bubbling, thermal treatment at a normal pressure or lowered pressure (0.1–0.2 bar) was applied on preforms. The most pronounced reduction of the number and size of the bubbles were obtained at 16 h at 50 °C and 0.1–0.2 bar.

4.2 *In situ* Polymerization Technique for ICPs

The main reason for using the *in situ* polymerization method is the poor processability of bulk polymerized PPy and PEDOT:PTS. It is problematic to obtain reproducible, homogeneous films with this method. It is especially difficult for *in situ* polymerization route carried out

for PPy since the placement of the substrate influences the amount of polymer precipitated or adsorbed on it. In the case of PEDOT, it can be controlled with the amount of polymerization solution that is deposited on the substrate. The uptake could be adjusted by the viscosity of the solution or by multiple coating cycles. Polymerization was successfully carried out on both planar sheets and fibers of PMMA. In the case of PPy we observed some problems. Since the polymer is mainly precipitated on the substrate there tended to be loose uneven agglomerates of PPy on PMMA substrates that were removed during the washing step. The poor mechanical properties of the coatings presented a real problem, especially for PPy films.

In the case of PEDOT:PTS the films were deposited by drop coating. The polymerization solution was evenly distributed on PMMA samples and the adhesion was good. This is because ethanol was used as a solvent that wets PMMA well. In the case of PPy, water was used as a solvent and no proper adhesion could be achieved with hydrophobic PMMA. Surfactants could have been used to enhance wetting, but those tend to influence the morphology of the PPy film as was demonstrated in [31, 107].

4.2.1 Polypyrrole

The main goal in the PPy study reported in article **II** was to optimize the preparation process of transparent thin film electrodes for practical applications. The main question was how to obtain a good conductivity versus transmittance ratio within a reasonably short processing time. The main results of those experiments are depicted in Fig. 4.1. During experimental work it was found out that the polymerization speed was higher in the case of path II. The reason for this can be explained by the differences in the oxidation strength of $FeCl_3$ and APS. The latter one is a stronger oxidant and reacts faster than $FeCl_3$. From a practical processing point of view, the polymerization time of 3 to 6 hours obtained from path I is not acceptable. The difference in conductivity for PPy prepared by different paths was approximately 2 kΩ/sq.

The better transparency/conductivity ratio was also achieved in the case of polymerization path II. The films prepared by path II with surface resistivity of approximately 6 kΩ/sq had a transmittance value (at $\lambda = 600$ nm) of around 75% at polymerization time 5–7 min. The PPy films prepared by path I had a surface resistivity varying between 4.2 and 7 kΩ/sq and

had transmittance values around 45% to 48% with corresponding polymerization times being 3 hours and 4 hours, respectively.

The polymerization path II showed that polymerization at +5 °C leads to a polymer with a higher conductivity than that prepared at RT. This can be explained with the reduced motion of molecules at the lower temperature enabling polymer chains to grow in a more compact manner. Another reason is that the low temperature is also slowing down the reactivity of the oxidant and hence hindering the over-oxidation phenomenon. For Path I the influence of temperature on surface resistivity is not that obvious, but this could be attributed to too short time ranges. $FeCl_3$ is initially a less active oxidant than APS, and this activity is further suppressed at lower temperatures, thus slowing down the reaction speed.

Figure 4.1 (b) shows that for longer reaction times the surface resistivity starts to increase. This phenomenon is called over-oxidation. It is especially pronounced for PPy synthesized at RT. Over-oxidation is a degradation process of ICPs, meaning that the doped sites (holes) are oxidized even further, resulting in cross-links between adjacent chains and formation of unwanted side or end groups (hydroxy, carboxyl etc. groups). Samples that were let polymerize for 1.5 h had also changed color from grayish black to reddish brown and became nonconductive.

We studied the aging of PPy films during a period of 4 weeks. This is a rather short time, but gives some data of the aging speed and nature. Slightly controversial results were obtained compared to those found in the literature [29, 30]. Generally it has been reported that smaller counter-ions like Cl^- more easily migrate from the PPy structure than bulkier counter-ions (e.g. like $PTSA^-$). Current research claims that ageing of PPy(Cl^-) is slower than that of PPy($PTSA^-$). After 4 weeks the surface resistivity of PPy(Cl^-) had increased by 20% compared to 33% growth for PPy($PTSA^-$). Still, those results show that PPy is rather unstable at normal ambient conditions, since humidity and air cause oxidation of the material. Hermetical packaging is expected to improve the stability at least to some extent.

As the aim of this research was to study PPy films for a transparent electrode application, it was important to study the surface morphology of those films. The requirements for good films are flat with an even surface in order to ensure proper adhesion and contact of the subsequent layers deposited on the transparent electrode.

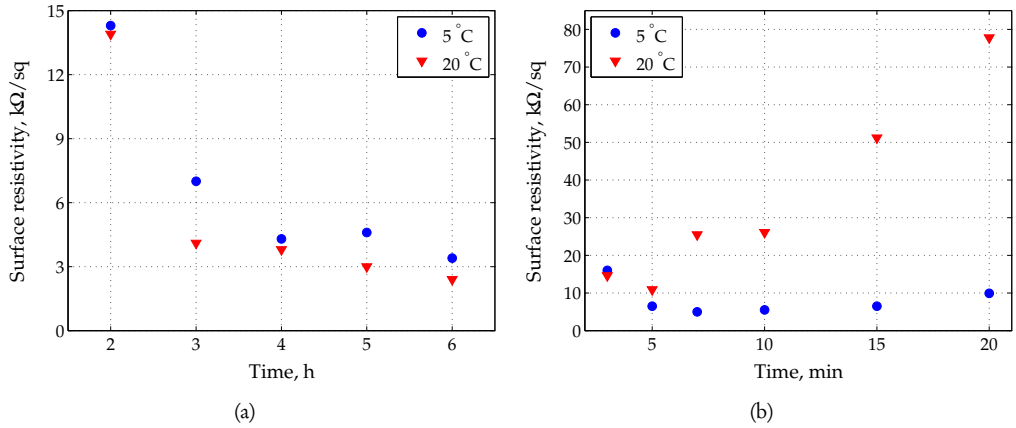

Figure 4.1 — Comparison between surface resistivity and optical absorbance ($\lambda = 600$ nm) of PPy films on PMMA substrate: (a) PPy prepared by Path I at +5 °C ; (b) PPy prepared by Path II at +5°C .

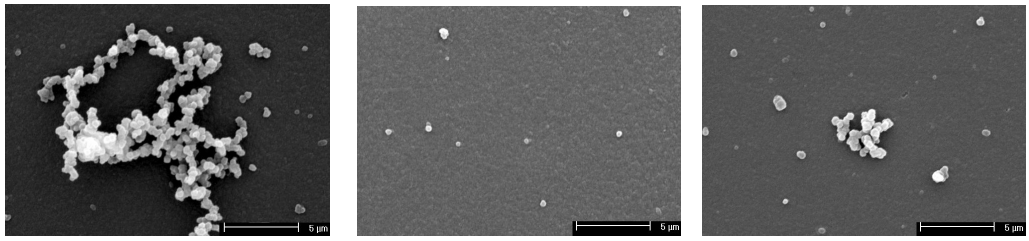

Figure 4.2 — Surface morphology of *in situ* polymerized PPy: (a) Path I, time 4 h, temperature 5 °C ; (b) Path I, time 5 h, temperature 5°C ; (c) Path II, time 7 min, temperature 5 °C .

The surface morphology examinations (Fig. 4.2) revealed that the surface of PPy is not completely flat, but there are some protrusions that are most likely polymerization centers. From Figures 4.2 (a) and (b) it can be seen that the surface becomes more even with a longer polymerization time. The film of PPy is precipitated on the substrate in the solution hence the position of the substrate has a crucial role in the film thickness and quality. The films shown in Fig. 4.2 were made on PMMA sheets placed vertically in the polymerization solution. This configuration should ensure more compact films than the horizontal placement of the substrate. The question of sample placement is especially crucial in the case of a fiber substrate. Otherwise, there was no difference observed between the film formation on either planar or cylindrical

substrates.

4.2.2 Poly(3,4-ethylenedioxythiophene)

The *In situ* polymerization of PEDOT was carried out by coating the polymerization mixture on a substrate. The polymerization was terminated by rinsing away the excess components with ethanol or water.

At the beginning the polymerization mixtures without pyridine were used, but this polymerization route led to a rapid oxidation reaction and subsequently to an over-oxidation. Normally-doped PEDOT looks dark blue, but over-oxidized PEDOT films looked black and have a lower conductivity than doped PEDOT.

PEDOT:PSS films were easy to prepare and demonstrated a high conductivity. The conductivity measurements of different PEDOT samples showed that the surface resistivity of PEDOT:PTS was 0.68 kΩ/sq, and PEDOT:PSS was 110 Ω/sq. Hence PEDOT has better conductivity than PPy.

The surface morphology studies made on the SEM showed that structures of PEDOT:PTS and PEDOT:PSS are different. The PEDOT:PTS (Fig. 4.3 (a)) formed a rather rough and porous film with pores of different sizes. On the other hand, the PEDOT:PSS (Fig. 4.3 (b)) formed a relatively smooth film with only very small pinholes. This phenomenon can be explained by the nature of counter ions used in these two polymers and is further discussed in Section 4.3.

4.3 PEDOT as an Ammonia Sensor

Several chemical sensors based on PEDOT were reviewed in section 2.3.5, but none of those works in the optical regime. It is a well known that ICPs have both an electrical and an optical response to the chemical changes of the ambient environment, but the extent of these two phenomena has not been compared.

The sensing mechanism of ICPs to NH_3 and other reactants (e.g. alcohols) is attributed to the π-conjugated system in the conductive polymer chain. Ammonia, as an electron donor, compensates the hole in the ICP chain by decreasing the polaron and/or bipolaron densities

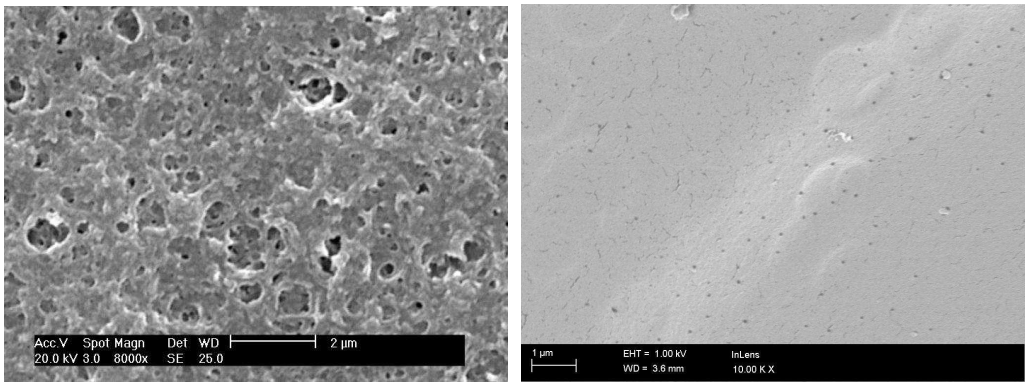

(a) (b)

Figure 4.3 — SEM images of (a) PEDOT:PTS and (b) PEDOT:PSS on PMMA sheets.

inside the band gap of the polymer. These modifications are expressed in both the electrical and optical properties of the conductive polymer [108]. Already in the very beginning of ICP research in 1977, it was observed that the vapors of NH_3 reduce the polyacetylene conductivity by more than four orders of magnitude [27].

The changes in the optical properties between the reduced and oxidized states can be seen from the UV-Vis spectra of PEDOT:PTS and PEDOT:PSS presented in Fig. 4.4. In its oxidized state PEDOT has a high concentration of free charge carriers thus indicating a good electrical conductivity, while the optical absorption is determined by transition between the polaronic states (high absorbance in the IR range). The increase in absorbance at 500–550 nm for a dedoped sample corresponds to a $\pi - \pi^*$ transition that can usually be seen as a strong peak at around 570–600 nm, but instead it is rather weak in this case referring only to partial dedoping. The spectrum of the dedoped PEDOT:PSS (Fig. 4.4 (b)) has a surprisingly high absorption. The origin of this phenomenon is not fully known, but it corresponds well with the spectra of reduced PEDOT:PSS, which are found in the literature [109].

In situ polymerized PEDOT:PTS can be used for detecting ammonia vapors in the concentration range of 135–1350 ppm in both the electrical and the optical regime. Active layers are easy to prepare and the processing techniques such as brush coating and dip-coating are compatible with the fiber architecture. PEDOT:PTS permits the construction of an optoelectronic fiber

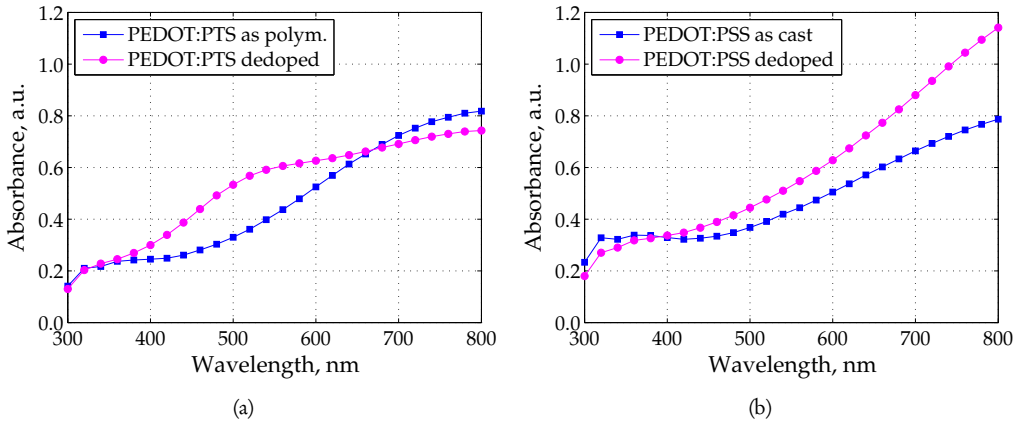

Figure 4.4 — UV-Vis spectra of (a) PEDOT:PTS and (b) PEDOT:PSS in the oxidized and partly reduced state.

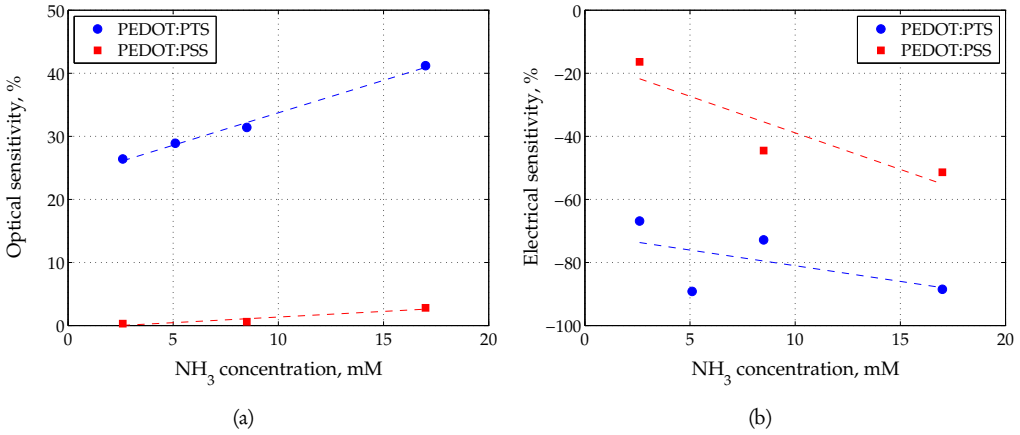

Figure 4.5 — (a) The optical and (b) the electrical sensitivity of PEDOT to ammonia.

sensor that would give both an electrical and an optical response. PEDOT:PSS gives an electrical response to ammonia (Fig. 4.5(b)), but it is weaker than for PEDOT:PTS. The films of PEDOT:PSS are easy to make, the processing is compatible with the fiber architecture, and the films are highly conductive. However, PEDOT:PSS demonstrates a weak optical response (Fig. 4.5(a)) to NH_3 in the visible range of light.

The attacking mechanism of NH_3 is based on its coordination to the pair of the hole and counter ion, hence changing the doping degree of PEDOT. The different PEDOT responses can be explained by their different molecular structures since the counter-ion is different. PSS is a water soluble polyelectrolyte that has a high molar mass (i.e. chain length). It has been suggested that the short PEDOT oligomers are attached along the PSS chain. The chains of PEDOT:PSS form gel particles, consisting of tangled PEDOT:PSS chains and water [81]. Long molecules of PSS cause steric hindrance in the material resulting in a lower sensitivity. Another aspect is that in the case of measuring analytes from aqueous solutions, the water is causing swelling in PEDOT:PSS that is additionally blocking the access of the analyte to PEDOT.

PEDOT:PTS on the other hand has rather small counter-ion molecules that makes it easier for the analyte to access it. X-ray diffraction studies have shown that oligomer/polymer chains of PEDOT form π-stacks. These stacks have a characteristic repeating distance that depends on the size of the counter-ions, which are incorporated between these π-stacks [63, 79–81]. The reaction mechanism here results from the molecules of analyte that penetrate between the π-stacks and coordinate with the counter-ions and holes. The number of replaced counter-ions depends on the concentration of the analyte.

From a practical point of view, the response time of a sensing element is a crucial characteristic. PEDOT:PTS responds to ammonia vapors already within 1 min, but the sensitivity values reported in this thesis have been measured after 5 min of exposure time. The repeatability of the PEDOT sensor was assured by redoping the PEDOT by rinsing it in 5M HCl.

There were also some drawbacks discovered in the experimental work and the analysis of the ammonia sensor. The preparation of an evanescent field fiber-optic sensor (1 mm POF) with a PEDOT active element was not successful. A plausible explanation would be that very little light penetrated into the PEDOT film.

The electrical measurement set-up should have been arranged in a different way. Our technique did not enable the best precision level possible in the electrical measurements because the electrode contacts were not permanent (for each measurement electrodes were pressed against the PEDOT layer, and the latter tended to break).

The exposure mechanism of NH_3 should have been different. Gas feeding into a closed chamber would have given a better precision level. In the current technique there is water vapor present. For the electrical measurements samples were kept at standard conditions (23±1 °C and 25±3% RH) for 24 h in order to avoid the side effects of humidity. However, a partial weakening of the ammonia influence may have taken place. Optical absorbance measurements with a similar set-up, except for pure water only, did not reveal any influence.

4.4 Photovoltaic Fiber

A photovoltaic fiber based on DSSC technology is a totally new concept and has never been demonstrated by other research groups. Bulk heterojunction photovoltaic cells have been demonstrated according to the same principle that light is propagating inside the fiber.

A typical J-V-curve of a photovoltaic fiber is depicted in Fig. 4.6. The current density of all the photovoltaic fibers was poor, ranging from 1.81 nA/cm^2 to 146 nA/cm^2. The open circuit voltage, V_{oc}, varied from 0.33 V to 0.5 V, which is quite close to the V_{oc} values for planar DSSC typically ranging from 0.6 V to 0.7 V V_{oc} for the same materials. Such parameters result in extremely low total power conversion efficiencies.

The main reason for this poor performance is in the quality of the TiO_2 layer of the fibers. According to the SEM images of the ALD-made TiO_2 films, these layers are rather compact and nonporous. But the porosity of the TiO_2 layer plays a very important role because the adsorption capacity of a dye directly depends on the porosity of TiO_2. Only dye molecules directly attached to the semiconductor surface are able to efficiently inject charge carriers (electrons) into the semiconductor with a quantum yield of more than 90%. Since the overall light absorption of a dye monolayer is very small, this limits the photocurrent efficiency with respect to the incident light to a value well below 1% [100]. The TiO_2 paste contains nanoparticles that are sintered together during the heat treatment at 450–500 °C in order to achieve proper neck-

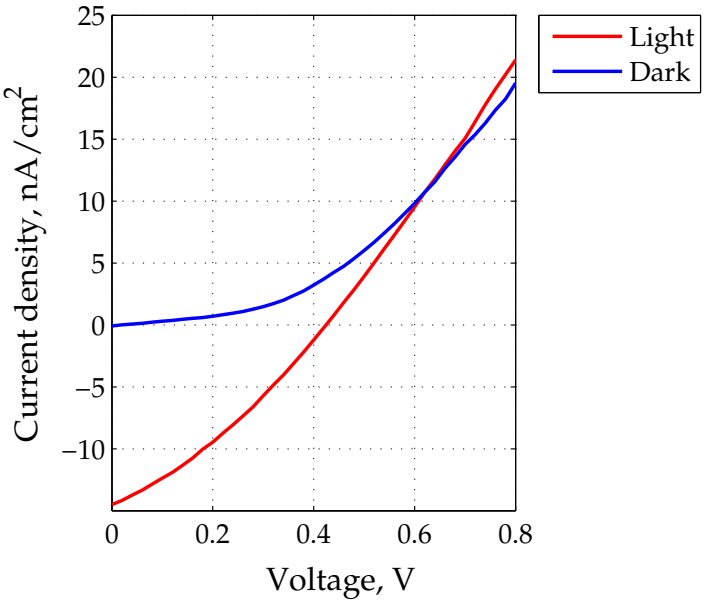

Figure 4.6 — Typical j-V-curve measured on a photovoltaic fiber in the dark and under illumination.

ing between the particles and to improve the film's adhesion to the substrate (Fig.4.7 (a)). The photoelectrode deposited by the ALD method yields in non-porous films (Fig.4.7 (b)), where only a very small amount of the dye can be adsorbed.

In our case the glass fiber based DSSCs performed worse than the POF based DSSCs. The adhesion of the sintered, porous TiO_2 layer on the glass fibers was rather poor, and roughly half of the layer detached during the rinsing. Typically, paste is applied by doctor-blading or screen-printing, which results in thin, even films. The adherence of these films to the substrate is good prior to the sintering because of the pressure was applied while the paste was spread. It is also possible that the surface energy and the surface properties of $SnO_2 : F$, which is the conductive coating typically used on DSSC glass substrates, are more favorable for TiO_2 adhesion, compared to those of ZnO:Al.

The contacts between different interfaces also play an important role in the cell performance. The charge carrier transport in organic electronic devices is strongly dependent on the molec-

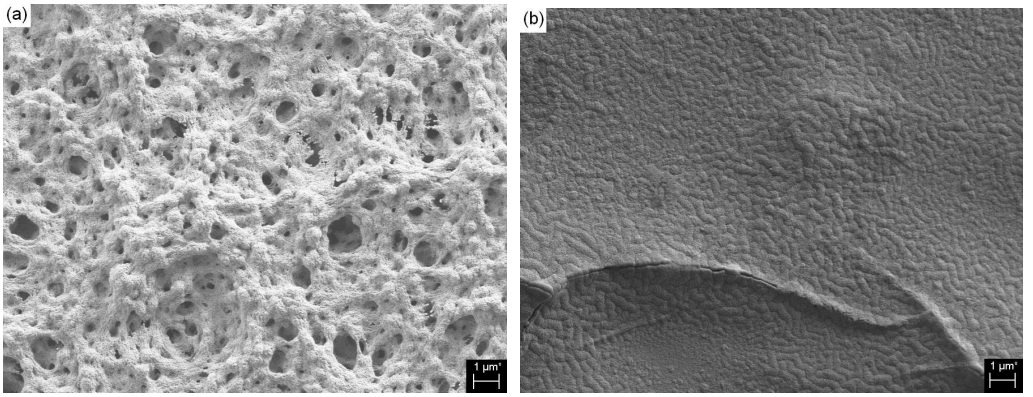

(a) (b)

Figure 4.7 — Surface morphology of the photoelectrode: (a) Nanoporous TiO_2 on glass fiber; (b) ALD coating on PMMA fiber: 130 nm of ZnO:Al on the bottom, 50 nm TiO_2 on top.

ular structure and the morphology of organic semiconductor materials [110]. The same phenomenon also holds true for DSSC. Charge-carrier mobilities are limited by the hopping process between the molecules in disordered regions of the material. If pressure is applied during the TiO_2 deposition, it ensures a closer contact between the particles of TiO_2 and the electrode. Although it was not investigated in this research, it can be assumed that the contact between the different material layers is not optimal because in the dip-coating no pressure is applied in the layer forming process.

It has been observed that the pressure between the different DSSC layers have influence on the cell performance [111]. This study investigated the influence of the pressure of counter electrode copper wires on cell performance. In the case of low interfacial pressure (0.02 N), the V_{oc} of the cell was large, but the I_{sc} was small. In order to obtain a high interfacial pressure (0.07 N), both the V_{oc} and I_{sc} were lowered. The optimal pressure was 0.04 N.

It is challenging to construct a multilayered structure mainly by dip-coating in a way that different layers would not mix together. All components such as the solvents and the processing temperatures have to be compatible with each other. If the solvent penetrates to the lower layers and dissolves it, it would short-circuit or cause the device malfunction. This could lead to low performance in the current case.

Another possible problem for poor performance of the photovoltaic fibers is the poor coupling of light into the photovoltaic structure. The poor coupling was also observed in the development of the evanescent field ammonia sensor. This conclusion can be drawn because the performance of the side-illuminated samples of the photovoltaic fibers performed better than the inside-illuminated fibers. The poor performance is most probably due to a too weak evanescent field that could be caused by the large diameter and high attenuation of the optical fibers. The angle of the incident light should not have been 0° as it was in our tests, but larger. The optimal incident angle would have been around 5 ° to 10 ° for that experiment [23]. Bending of the fiber would have increased the amount of incident light; however, this is not practically feasible.

The stability of the photovoltaic fiber is also an important issue. DSSC contains an electrolyte that has to be sealed in order to prevent drying. The devices prepared in this research had a very limited life time due to the evaporation of the electrolyte. Encapsulation with liquid materials like epoxy-based polymers would on the other hand cause problems because it is very likely to penetrate to the active structure. Conclusively, individually made films would provide a more favorable solution.

CHAPTER 5

Concluding Remarks

POF manufacturing methods used in this research did not yield data communication fibers of satisfactory quality. In preform manufacturing the feeding arrangement of raw materials and in the case of extrusion, the impurities of the pellets and the feeding system caused problems. However, extruded fibers are suitable for lighting and simple optical sensors (e.g. counters). The preform technology should be utilized for data communication fibers.

Electrical conductivity versus optical transmittance properties of PPy were studied for possible transparent electrode applications. The *in situ* deposition method was chosen because PPy is not soluble in any common solvents that could be easily used in the manufacturing environment. The *in situ* polymerization of PPy is an easy and straightforward process. The time scale is compatible with mass production (i.e. true for Path II). The resulting film quality is quite smooth and even, but it might be insufficient for thin film electronic devices. The electrical conductivity is also rather low (approximately 5–6 kΩ/sq) for real electronic applications. The most significant disadvantage of PPy however is its poor long term stability. PPy is not suitable for use in electronic devices as a transparent electrode mainly due to the poor conductivity. It is not practical to use as an antistatic coatings because it is not environmentally stable, and the packaging would ruin the coating effect.

PEDOT was demonstrated as an optical sensing element for ammonia sensing. The sensitivity depends on the nature of the counter-ion of PEDOT. PEDOT:PSS is not suitable for ammonia sensor applications because the PSS counter-ion blocks the diffusion of the analyte. PEDOT:PSS demonstrated a clear electrical response to NH_3, but PEDOT:PTS also had a higher sensitivity in this regime. In the *in situ* polymerization of PEDOT:PTS, the polymer chains

build up randomly on the substrate, which results in a material with a high surface area. This is always favorable when talking about sensor applications. Commercially-available PEDOT:PSS is easier to use, and, for example, it could be used in printable electrical sensors. The *in situ* polymerization of PEDOT:PTS is a simple technique, but it may be problematic to obtain a reproducible film quality. Furthermore, the adhesion to the substrate is sometimes poor.

Demonstration of a fiber-optic evanescent field sensor was not successful. The main reason for this is most plausible due to the low strength of the evanescent field penetrating into the cladding of the plastic optical fiber of a large diameter. Additionally, the high attenuation of POF diminishes the small evanescent field even further. Still it is possible to use an optical sensor consisting of planar sensing elements of PEDOT and optical fibers. In principal, PEDOT as well as other ICPs in sensor applications have poor selectivity as they are sensitive to any reducing or oxidizing agent. The selectivity could be enhanced by using protective membranes or by further chemical modification of PEDOT.

DSSC deposited on an optical fiber has not been demonstrated before. However, the poor performance of the photovoltaic fiber is a problem. The main reason for this is the low porosity of TCO and hence the low adsorption of dye molecules in the case of a POF substrate. In the case of SOF, the layer of nanoporous TiO_2 was too thick, which peeled off during washing. It is possible that there was a rather poor adhesion between the substrate oxide and TiO_2. Most probably the dip-coating of TiO_2 paste should be optimized (thinner composition, multiple dippings). The long term stability of photovoltaic fibers is also problematic as the evaporation of the electrolyte leads to failure. Such photovoltaic fibers would need hermetic packaging.

This thesis demonstrates that the chemical and physical sensors can be built on flexible plastic optical fibers. In cerain applications SOF should be preferred due to the limitation of POF in thermal properties and optical transmission. Building a functional optical fiber is not an easy task. After the studies presented in this thesis, it can be concluded that it is challenging to make multilayered optoelectronic devices on optical fibers. One of the biggest problems is that if different layers are deposited by dip-coating, the inner layers are easily destroyed by the solvents. Also, the organic electronic materials (especially those available in liquid form) tend to have a poorer performance than their solid counterparts. A new set of manufacturing technologies could reveal other perspectives on manufacturing possibilities. Two possibilities

are VPP for polymer layers, and ALD for metal and metal oxide layers. The ALD method ensures the layer smoothness and thickness. A high pressure treatment is needed to enhance the contact at the layer interface.

CHAPTER **6**

Summary of the Publications and the Author's Contribution

This thesis is based on five original publications dealing with different areas of fiber-optic active structures. Publication **I** deals with optical fiber manufacturing questions. Publications **II - III** mainly deal with the synthesis and characterization of different electrically conductive polymers. Publication **IV** compares the electrical and optical sensitivity of a certain electrically conductive polymer. In **V** a hybrid photovoltaic structure is demonstrated on an optical fiber.

In publication **I** we discussed the manufacturing methods for MSI POFs and demonstrated the practical results. Our preform manufacturing is realized by thermal polymerization and photopolymerization. We obtained a good quality preform only using thermal polymerization. Our two layer extrusion was tested for obtaining SI optical fibers consisting of a PMMA core and PC cladding. We drew fibers using IR lamps for preform melting. The commercial preforms we used, exhibited problems with residual monomers and other low molecular compounds causing extensive bubbling in preforms leading to a low quality optical fiber. The author performed the analysis of experimental results and wrote the article.

In publication **II** we studied the chemical *in situ* polymerization of PPy on planar and fibrous PMMA substrates is studied. We compared two polymerization paths using $FeCl_3$ oxidant and the other using APS combined with PTSA. We demonstrated the influence of polymerization time, temperature, and oxidant on conductivity of PPy. We showed the relationship between the electrical conductivity and optical transmission properties of PPy films. We reported the results of ageing tests of PPy films. I performed all the experimental work and wrote the article.

In publication **III** we concentrate on the *in situ* synthesis and characterization of optical properties of PEDOT films. We demonstrated the use of PEDOT as an optical sensing element in

measuring ammonia vapors. We found that the sensing mechanism of PEDOT is based on the changes in optical absorption properties caused by the variations in redox states in the presence of ammonia. We observed a linear relationship between the optical sensitivity and ammonia concentration in the range of 135-1350 ppm. We showed the repeatability of the PEDOT sensing element. I carried out all the experimental work and wrote the article.

We continue studying PEDOT for measuring ammonia in publication **IV**, where the research is focused on comparison between the electrical and optical sensitivity of PEDOT to ammonia. We are considering the difference between the *in situ* polymerized PEDOT and commercially available PEDOT. We observed that the electrical sensitivity of PEDOT to ammonia was bigger than the optical sensitivity. We found that *in situ* PEDOT demonstrated higher sensitivity than commercial PEDOT. Additionally, we found that the optical sensitivity of commercial PEDOT was low, but the electrical sensitivity was clearly observable. I made all the experimental work and wrote the article.

In publication **V** we built a hybrid optoelectronic structure on an optical fiber converting light modes propagating in the optical fiber into an electrical signal. We used silica and plastic optical fibers without cladding. We compensated the cladding layer of the fibers with a DSSC structure. Our resulting fibers are referred to as photovoltaic fibers. We demonstrated J-V-curves, fill factor, and total power conversion efficiency of PV fibers. I made the theoretical design of PV fibers and the measurement scheme, participated in the experimental work, and wrote approximately one third of the article.

Bibliography

[1] E. Reichmanis, H. Katz, C. Kloc, and A. Maliakal. Plastic Electronic Devices: From Materials Design to Device Applications. *Bell Labs Technical Journal*, **10** (2005) 87–105.

[2] W. Daum, J. Krauser, P. E. Zamzow, and O. Ziemann. *POF — Polymer Optical Fibers for Data Communication*. Springer, 2002.

[3] T. Ishigure, Y. Koike, and J. Fleming. Optimum Index Profile of the Perfluorinated Polymer-Based GI Polymer Optical Fiber and its Dispersion Properties. *J. Lightwave Technol.*, **18** (2000) 178–184.

[4] Y. Koike, T. Ishigure, and E. Nihei. High-Bandwidth Graded-Index Polymer Optical Fiber. *J. Lightwave Technol.*, **13** (1995) 1475–1489.

[5] B.-G. Shin, J.-H. Park, and J.-J. Kim. Low-Loss, High-Bandwidth Graded-Index Plastic Optical Fiber Fabricated by the Centrifugal Deposition Method. *Appl. Phys. Lett.*, **82** (2003) 4645–4647.

[6] A. Weinert. *Plastic Optical Fibers*. Publicis MCD Verlag, 1999.

[7] M. Asai, R. Hirose, A. Kondo, and Y. Koike. High-Bandwidth Graded-Index Plastic Optical Fiber by the Dopant Diffusion Coextrusion Process. *J. Lightwave Technol.*, **25** (2007) 3062–3067.

[8] J. Zubia, O. Aresti, J. Arrue, and M. Lopez-Amo. Barrier Sensor Based on Plastic Optical Fiber to Determine the Wind Speed at a Wind Generator. *IEEE J. Sel. Top. Quantum Electron.*, **6** (2000) 773–779.

[9] C. Vázquez, A. B. Gonzalo, S. Vargas, and J. Montalvo. Multi-Sensor System Using Plastic Optical Fibers for Intrinsically Safe Level Measurements. *Sens. Actuators, A, Phys*, **116** (2004) 22–32.

[10] A. Paz, J. Acevedo, J. Gandoy, A. del Vazquez, C.-P. Freire, and M. Soria. Plastic Optical Fiber Sensor for Real Time Density Measurements in Wine Fermentation. *IEEE Instrumentation and Measurement Technology Conference Proceedings*, 1–5.

[11] R. M. Ribeiro, J. L. P. Canedo, M. M. Werneck, and L. R. Kawase. An Evanescent-Coupling Plastic Optical Fibre Refractometer and Absorptionmeter Based on Surface Light Scattering. *Sens. Actuators, A, Phys*, **101** (2002) 69–76.

[12] E. Alvarado-Méndez, R. Rojas-Laguna, J. Andrade-Lucio, D. Hernández-Cruz, R. Lessard, and J. Aviña-Cervantes. Design and Characterization of pH Sensor Based on Sol-Gel Silica Layer on Plastic Optical Fiber. *Sens. Actuators, B, Chem*, **106** (2005) 518–522.

[13] T. Brook, M. Taib, and R. Narayanaswamy. Extending the Range of a Fibre-Optic Relative-Humidity Sensor. *Sens. Actuators, B, Chem*, **39** (1997) 272–276.

[14] E. J. Netto, J. I. Peterson, M. McShane, and V. Hampshire. A Fiber-Optic Broad-Range pH Sensor System for Gastric Measurements. *Sens. Actuators, B, Chem*, **29** (1995) 157–163.

[15] S. V. Frolov, A. Fujii, D. Chinn, Z. V. Vardeny, K. Yoshino, and R. V. Gregory. Cylindrical Microlasers and Light Emitting Devices From Conducting Polymers. *Appl. Phys. Lett.*, **72** (1998) 2811–2813.

[16] J. Wang and K. Wong. Polarization Characteristics of a Light-Emitting Polymer Microring Laser. *Appl. Phys. B*, **87** (2007) 685–691.

[17] H. Tsuda and J.-R. Lee. Strain and Damage Monitoring of CFRP in Impact Loading Using a Fiber Bragg Grating Sensor System. *Compos. Sci. Technol.*, **67** (2007) 1353–1361.

[18] L. Dziuda, G. Fusiek, P. Niewczas, G. Burt, and J. McDonald. Laboratory Evaluation of the Hybrid Fiber-Optic Current Sensor. *Sens. Actuators, A, Phys*, **136** (2006) 184–190.

[19] A. Rose, Z. Zhu, C. F. Madigan, T. M. Swager, and V. Bulovic. Sensitivity Gains in Chemosensing by Lasing Action in Organic Polymers. *Nature*, **434** (2005) 876–879.

[20] M. Bayindir, O. Shapira, D. Saygin-Hinczewski, J. Viens, A. F. Abouraddy, J. D. Joannopoulos, and Y. Fink. Integrated Fibres for Self-Monitored Optical Transport. *Nat. Mater.*, **4** (2005) 820–825.

[21] M. Bayindir, F. Sorin, A. F. Abouraddy, J. Viens, S. D. Hart, J. D. Joannopoulos, and Y. Fink. Metal-Insulator-Semiconductor Optoelectronic Fibres. *Nature*, **431** (2004) 826–829.

[22] P. J. A. Sazio, A. Amezcua-Correa, C. E. Finlayson, J. R. Hayes, T. J. Scheidemantel, N. F. Baril, B. R. Jackson, D.-J. Won, F. Zhang, E. R. Margine, V. Gopalan, V. H. Crespi, and J. V. Badding. Microstructured Optical Fibers as High-Pressure Microfluidic Reactors. *Science*, **311** (2006) 1583–1586.

[23] J. Liu, M. A. G. Namboothiry, and D. L. Carroll. Fiber-Based Architectures for Organic Photovoltaics. *Appl. Phys. Lett.*, **90** (2007) 063501.

[24] G. Benoit, S. Hart, B. Temelkuran, J. Joannopoulos, and Y. Fink. Static and Dynamic Properties of Optical Microcavities in Photonic Bandgap Yarns. *Adv. Mater.*, **15** (2003) 2053–2056.

[25] W. F. Lowe, L. J. Button, and R. E. Slovacek. *Biosensors with Fiberoptics*, chapter Optical Characteristics of Fiber Optics Evanescent Wave Sensors, 139–180. Humana Press, Clifton, NJ, 1991.

[26] G. Boisde and A. Harmer. *Chemical and Biochemical Sensing with Optical Fibers and Waveguides*. Artech House, 1996.

[27] C. K. Chiang, C. R. Fincher, Y. W. Park, A. J. Heeger, H. Shirakawa, E. J. Louis, S. C. Gau, and A. G. MacDiarmid. Electrical Conductivity in Doped Polyacetylene. *Phys. Rev. Lett.*, **39** (1977) 1098–1101.

[28] A. Malinauskas. Chemical Deposition of Conducting Polymers. *Polymer*, **42** (2001) 3957–3972.

[29] M. M. Chehimi and E. Abdeljalil. A Study of The Degradation and Stability of Polypyrrole by Inverse Gas Chromatography, X-Ray Photoelectron Spectroscopy, and Conductivity Measurements. *Synth. Met.*, **145** (2004) 15–22.

[30] J. Thiéblemont, M. Planche, C. Petrescu, J. Bouvier, and G. Bidan. Stability of Chemically Synthesized Polypyrrole Films. *Synth. Met.*, **59** (1993) 81–96.

[31] S. H. Cho, K. T. Song, and J. Y. Lee. *Handbook of Conducting Polymers: Conjugated Polymers*, chapter 8 Recent Advances in Polypyrrole, 8–1–8–87. CRC Press, 2007.

[32] P. A. Kilmartin and G. A. Wright. Photoeffects to Characterise Polypyrrole Electrodes and Bilayers with Polyaniline. *Electrochim. Acta*, **46** (2001) 2787–2794.

[33] M. Sak-Bosnar, M. V. Budimir, S. Kovac, D. Kukulj, and L. Duic. Chemical and Electrochemical Characterization of Chemically Synthesized Conducting Polypyrrole. *J. Polym. Sci., A, Polym. Chem.*, **30** (1992) 1609–1614.

[34] J. Reut. *Polypyrrole Coatings on Conducting and Insulating Substrates*. Ph.D. thesis, Tallinn University of Technology, 2004.

[35] J. Kim, D. Sohn, Y. Sung, and E.-R. Kim. Fabrication and Characterization of Conductive Polypyrrole Thin Film Prepared by in situ Vapor-Phase Polymerization. *Synth. Met.*, **132** (2003) 309–313.

[36] D. S. Kumar, K. Nakamura, S. Nishiyama, S. Ishii, H. Noguchi, K. Kashiwagi, and Y. Yoshida. Optical and Electrical Characterization of Plasma Polymerized Pyrrole Films. *J. Appl. Phys.*, **93** (2003) 2705–2711.

[37] K. Hosono, I. Matsubara, N. Murayama, W. Shin, N. Izu, and S. Kanzaki. Structure and Properties of Plasma Polymerized and 4-Ethylbenzenesulfonic Acid-Doped Polypyrrole Films. *Thin Solid Films*, **441** (2003) 72–75.

[38] J. Wang, K. G. Neoh, and E. T. Kang. Comparative Study of Chemically Synthesized and Plasma Polymerized Pyrrole and Thiophene Thin Films. *Thin Solid Films*, **446** (2004) 205–217.

[39] A. J. Heeger, S. Kivelson, J. R. Schrieffer, and W. P. Su. Solitons in Conducting Polymers. *Rev. Mod. Phys.*, **60** (1988) 781–850.

[40] D. Beljonne, J. Cornil, V. Coropceanu, D. A. da Silva Filho, V. Geskin, R. Lazzaroni, P. Leclère, and J.-L. Brédas. *Handbook of Conductive Polymers — Conjugated Polymers*, chapter 1 On the Transport, Optical, and Self-Assembly Properties of π-Conjugated Materials: A Combined Theoretical/Experimental Insight, 1–3–1–46. CRC Press, 2007.

[41] L. Zuppiroli, M. N. Bussac, S. Paschen, O. Chauvet, and L. Forro. Hopping in Disordered Conducting Polymers. *Phys. Rev. B*, **50** (1994) 5196–5203.

[42] A. N. Aleshin, S. R. Williams, and A. J. Heeger. Transport Properties of Poly(3,4-ethylenedioxythiophene)/Poly(styrenesulfonate). *Synth. Met.*, **94** (1998) 173–177.

[43] Y. Shen and M. Wan. *In situ* Doping Polymerization of Pyrrole With Sulfonic Acid as a Dopant. *Synth. Met.*, **96** (1998) 127–132.

[44] S. Garreau, G. Louarn, J. Buisson, G. Froyer, and S. Lefrant. In Situ Spectroelectrochemical Raman Studies of Poly(3,4-ethylenedioxythiophene) (PEDT). *Macromolecules*, **32** (1999) 6807–6812.

[45] X. Chen and O. Inganas. Three-Step Redox in Polythiophenes: Evidence from Electrochemistry at an Ultramicroelectrode. *J. Phys. Chem.*, **100** (1996) 15202–15206.

[46] R. Gregory, W. Kimbrell, and H. Kuhn. Conductive textiles. *Synth. Met.*, **28** (1989) 823–835.

[47] G. J. Cruz, J. Morales, and R. Olayo. Films Obtained by Plasma Polymerization of Pyrrole. *Thin Solid Films*, **342** (1999) 119–126.

[48] S. N. Tan and H. Ge. Investigation Into Vapour-Phase Formation of polypyrrole. *Polymer*, **37** (1996) 965–968.

[49] Y. Kudoh. Properties of Polypyrrole Prepared by Chemical Polymerization Using Aqueous Solution Containing $Fe_2(SO_4)_3$ and Anionic Surfactant. *Synth. Met.*, **79** (1996) 17–22.

[50] M. Morita, I. Hashida, and M. Nishimura. Conducting Polypyrrole Composite Thin Films Chemically Prepared by Spreading on Surface of Aqueous Solution Containing Oxidizing Agent. *J. Appl. Polym. Sci.*, **36** (1988) 1639–1650.

[51] M. Omastová, J. Pavlinec, J. Pionteck, F. Simon, and S. Košina. Chemical Preparation and Characterization of Conductive Poly(Methyl Methacrylate)/Polypyrrole Composites. *Polymer*, **39** (1998) 6559–6566.

[52] J. Jang, M. Chang, and H. Yoon. Chemical Sensors Based on Highly Conductive Poly(3,4-ethylenedioxythiophene) Nanorods. *Adv. Mater.*, **17** (2005) 1616–1620.

[53] R. A. Zoppi, M. I. Felisberti, and M.-A. D. Paoli. Chemical preparation of conductive elastomeric blends: Polypyrrole/EPDM. I. Oxidant particle-size effect. *J. Polym. Sci., Part A: Polym. Chem.*, **32** (1994) 1001–1008.

[54] J.-W. Park, J.-H. Lee, J.-Y. Lee, S.-I. Kho, and T.-W. Kim. Characteristics of Organic Electroluminescent Devices Using Polypyrrole Conducting Layer and Undoped Conjugated Polymer Layer. *Thin Solid Films*, **363** (2000) 259–262.

[55] R. Cervini, Y. Cheng, and G. Simon. Solid-State Ru-Dye Solar Cells Using Polypyrrole as a Hole Conductor. *J. Phys. D: Appl. Phys.*, **37** (2004) 13–20.

[56] L. Bansal and M. El-Sherif. Intrinsic Optical-Fiber Sensor for Nerve Agent Sensing. *IEEE Sensors J.*, **5** (2005) 648–655.

[57] H.-K. Jun, Y.-S. Hoh, B.-S. Lee, S.-T. Lee, J.-O. Lim, D.-D. Lee, and J.-S. Huh. Electrical Properties of Polypyrrole Gas Sensors Fabricated Under Various Pretreatment Conditions. *Sens. Actuators, B, Chem*, **96** (2003) 576–581.

[58] Y. Li, X. Cheng, M. Leung, J. Tsang, X. Tao, and M. Yuen. A Flexible Strain Sensor from Polypyrrole-Coated Fabrics. *Synth. Met.*, **155** (2005) 89–94.

[59] C. Y. Lee, D. E. Lee, J. Joo, M. S. Kim, J. Y. Lee, S. H. Jeong, and S. W. Byun. Conductivity and EMI Shielding Efficiency of Polypyrrole and Metal Compounds Coated on Nonwoven Fabrics. *Synth. Met.*, **119** (2001) 429–430.

[60] E. Gasana, P. Westbroek, J. Hakuzimana, K. De Clerck, G. Priniotakis, P. Kiekens, and D. Tseles. Electroconductive Textile Structures Through Electroless Deposition of Polypyrrole and Copper at Polyaramide Surfaces. *Surf. Coat. Technol.*, **201** (2006) 3547–3551.

[61] B. Kim, V. Koncar, E. Devaux, C. Dufour, and P. Viallier. Electrical and Morphological Properties of PP and PET Conductive Polymer Fibers. *Synth. Met.*, **146** (2004) 167–174.

[62] A. Harlin, P. Nousiainen, A. Puolakka, J. Pelto, and J. Sarlin. Development of Polyester and Polyamide Conductive Fibre. *J. Mater. Sci.*, **40** (2005) 5365–5371.

[63] L. Pettersson, T. Johansson, F. Carlsson, H. Arwin, and O. Inganas. Anisotropic Optical Properties of Doped Poly(3,4-Ethylenedioxythiophene). *Synth. Met.*, **101** (1999) 198–199.

[64] A. Kros, N. A. Sommerdijk, and R. J. Nolte. Poly(pyrrole) Versus Poly(3,4-Ethylenedioxythiophene): Implications for Biosensor Applications. *Sens. Actuators, B, Chem*, **106** (2005) 289–295.

[65] Y. Kudoh, K. Akami, H. Kusayanagi, and Y. Matsuya. Chemical Polymerization of 3,4-ethylenedioxythiophene in an Aqueous Medium Containing a Phenol Derivative as an Additive. *Synth. Met.*, **123** (2001) 541–544.

[66] M. Dietrich, J. Heinze, G. Heywang, and F. Jonas. Electrochemical and Spectroscopic Characterization of Polyalkylenedioxythiophenes. *J. Electroanal. Chem.*, **369** (1994) 87–92.

[67] Q. Pei, G. Zuccarello, M. Ahlskog, and O. Inganäs. Electrochromic and Highly Stable Poly(3,4-Ethylenedioxythiophene) Switches Between Opaque Blue-Black and Transparent Sky Blue. *Polymer*, **35** (1994) 1347–1351.

[68] J. C. Carlberg and O. Inganäs. Fast Optical Spectroscopy of the Electrochemical Doping of Poly(3,4-ethylenedioxythiophene). *J. Electrochem. Soc.*, **145** (1998) 3810–3814.

[69] D. M. de Leeuw, P. A. Kraakman, P. F. G. Bongaerts, C. M. J. Mutsaers, and D. B. M. Klaassen. Electroplating of Conductive Polymers for the Metallization of Insulators. *Synth. Met.*, **66** (1994) 263–273.

[70] B. Winther-Jensen and K. West. Vapor-Phase Polymerization of 3,4-Ethylenedioxythiophene: A Route to Highly Conducting Polymer Surface Layers. *Macromolecules*, **37** (2004) 4538–4543.

[71] B. Winther-Jensen, D. W. Breiby, and K. West. Base Inhibited Oxidative Polymerization of 3,4-Ethylenedioxythiophene With Iron(III)tosylate. *Synth. Met.*, **152** (2005) 1–4.

[72] J. Lock, S. Im, and K. Gleason. Oxidative Chemical Vapor Deposition of Electrically Conducting Poly(3,4-ethylenedioxythiophene) Films. *Macromolecules*, **39** (2006) 5326–5329.

[73] R. Corradi and S. Armes. Chemical Synthesis of Poly(3,4-Ethylenedioxythiophene). *Synth. Met.*, **84** (1997) 453–454.

[74] Y. Kudoh, K. Akami, and Y. Matsuya. Chemical Polymerization of 3,4-Ethylenedioxythiophene Using an Aqueous Medium Containing an Anionic Surfactant. *Synth. Met.*, **98** (1998) 65–70.

[75] T. Y. Kim, C. M. Park, J. E. Kim, and K. S. Suh. Electronic, Chemical and Structural Change Induced by Organic Solvents in Tosylate-Doped Poly(3,4-ethylenedioxythiophene) (PEDOT-OTs). *Synth. Met.*, **149** (2005) 169–174.

[76] Clevios^{TM} P Formulation Guide. 2008. URL http://www.baytron.com/medien/dokumente/document_20_clevios_form_guide_web.pdf.

[77] L. Groenendaal, F. Jonas, D. Freitag, H. Pielartzik, and J. R. Reynolds. Poly(3,4-ethylenedioxythiophene) and Its Derivatives: Past, Present, and Future. *Adv. Mater.*, **12** (2000) 481–494.

[78] K. Aasmundtveit, E. Samuelsen, L. Pettersson, O. Inganas, T. Johansson, and R. Feidenhans'l. Structure of Thin Films of Poly(3,4-ethylenedioxythiophene). *Synth. Met.*, **101** (1999) 561–564.

[79] L. A. A. Pettersson, F. Carlsson, O. Inganas, and H. Arwin. Spectroscopic Ellipsometry Studies of the Optical Properties of Doped Poly(3,4-Ethylenedioxythiophene): an Anisotropic Metal. *Thin Solid Films*, **313-314** (1998) 356–361.

[80] L. A. A. Pettersson, S. Ghosh, and O. Inganäs. Optical Anisotropy in Thin Films of Poly(3,4-Ethylenedioxythiophene)-Poly(4-Styrenesulfonate). *Org. Electron.*, **3** (2002) 143–148.

[81] S. Kirchmeyer, K. Reuter, and J. C. Simpson. *Handbook of Conducting Polymers — Conjugated Polymers*, chapter 10 Poly(3,4-Ethylenedioxythiophene)—Scientific Importance, Remarkable Properties, and Applications, 10–1–10–22. CRC Press, 2007.

[82] Y. Saito, T. Kitamura, Y. Wada, and S. Yanagida. Poly(3,4-Ethylenedioxythiophene) as a Hole Conductor in Solid State Dye Sensitized Solar Cells. *Synth. Met.*, **131** (2002) 185–187.

[83] B. Winther-Jensen and F. C. Krebs. High-Conductivity Large-Area Semi-Transparent Electrodes for Polymer Photovoltaics by Silk Screen Printing and Vapour-Phase Deposition. *Sol. Energ. Mater. Sol. Cells*, **90** (2006) 123–132.

[84] K. H. Hong, K. W. Oh, and T. J. Kang. Preparation and Properties of Electrically Conducting Textiles by *in situ* Polymerization of Poly(3,4-ethylenedioxythiophene). *J. Appl. Polym. Sci.*, **97** (2005) 1326–1332.

[85] W. A. Daoud, J. H. Xin, and Y. S. Szeto. Polyethylenedioxythiophene Coatings for Humidity, Temperature and Strain Sensing Polyamide Fibers. *Sens. Actuators, B, Chem*, **109** (2005) 329–333.

[86] J. Ouyang and Y. Yang. Conducting Polymer as Transparent Electric Glue. *Adv. Mater.*, **18** (2006) 2141–2144.

[87] M. S. Lee, H. S. Kang, H. S. Kang, J. Joo, A. J. Epstein, and J. Y. Lee. Flexible All-Polymer Field Effect Transistors with Optical Transparency Using Electrically Conducting Polymers. *Thin Solid Films*, **477** (2005) 169–173.

[88] H. Rost, J. Ficker, J. S. Alonso, L. Leenders, and I. McCulloch. Air-Stable All-Polymer Field-Effect Transistors With Organic Electrodes. *Synth. Met.*, **145** (2004) 83–85.

[89] M. Ando, C. Swart, E. Pringsheim, V. M. Mirsky, and O. S. Wolfbeis. Optical Ozone-Sensing Properties of Poly(2-Chloroaniline), Poly(N-Methylaniline) and Polyaniline Films. *Sens. Actuators, B, Chem*, **108** (2005) 528–534.

[90] Z. Jin, Y. Su, and Y. Duan. Development of a Polyaniline-Based Optical Ammonia Sensor. *Sens. Actuators, B, Chem*, **72** (2001) 75–79.

[91] J. Elizalde-Torres, H. Hu, and A. García-Valenzuela. NO_2-Induced Optical absorbance changes in Semiconductor Polyaniline Thin Films. *Sens. Actuators, B, Chem*, **98** (2004) 218–226.

[92] I. Lahdesmaki, W. W. Kubiak, A. Lewenstam, and A. Ivaska. Interferences in a Polypyrrole-Based Amperometric Ammonia Sensor. *Talanta*, **52** (2000) 269–275.

[93] K. H. Hong, K. W. Oh, and T. J. Kang. Polyaniline-Nylon 6 Composite Fabric for Ammonia Gas Sensor. *J. Appl. Polym. Sci.*, **92** (2004) 37–42.

[94] S. Christie, E. Scorsone, K. Persaud, and F. Kvasnik. Remote Detection of Gaseous Ammonia Using the Near Infrared Transmission Properties of Polyaniline. *Sens. Actuators, B, Chem*, **90** (2003) 163–169.

[95] M. F. Mabrook, C. Pearson, and M. C. Petty. An Inkjet-Printed Chemical Fuse. *J. of Phys: Conf. Ser.*, **15** (2005) 39–44.

[96] K.-C. Ho, W.-M. Yeh, T.-S. Tung, and J.-Y. Liao. Amperometric Detection of Morphine Based on Poly(3,4-ethylenedioxythiophene) Immobilized Molecularly Imprinted Polymer Particles Prepared by Precipitation Polymerization. *Anal. Chim. Acta*, **542** (2005) 90–96.

[97] T. A. Bendikov and T. C. Harmon. Long-Lived Solid State Perchlorate Ion Selective Sensor Based on Doped Poly(3,4-ethylenedioxythiophene) (PEDOT) Films. *Anal. Chim. Acta*, **551** (2005) 30–36.

[98] J. Liu, M. Agarwal, K. Varahramyan, E. S. Berney IV, and W. D. Hodo. Polymer-Based Microsensor for Soil Moisture Measurement. *Sens. Actuators, B, Chem*, **129** (2008) 599–604.

[99] M. Grätzel. Dye-Sensitized Solar Cells. *J. Photochem. Photobiol., C*, **4** (2003) 145–153.

[100] A. Goetzberger, C. Hebling, and H.-W. Schock. Photovoltaic Materials, History, Status and Outlook. *Mater. Sci. Eng., R*, **40** (2003) 1–46.

[101] T. N. Murakami and M. Grätzel. Counter Electrodes for DSC: Application of Functional Materials as Catalysts. *Inorg. Chim. Acta*, **361** (2008) 572–580.

[102] SFS-EN 1149-1 Protective Clothing. Electrostatic properties. Part 1: Surface resistivity, 2006.

[103] J. Paasi. Surface Resistance or Surface Resistivity. Technical report, VTT, 2002.

[104] R. W. Berry, P. M. Hall, and M. T. Harris. *Thin Film Technology*. Van Nostrand Reinhold Company, New York, 1968.

[105] H. C. Starck. *Measuring Method for Determining the Surface Resistivity of Clevios Coatings*, 2008.

[106] B. P. Rand, J. Genoe, P. Heremans, and J. Poortmans. Solar Cells Utilizing Small Molecular Weight Organic Semiconductors. *Prog. Photovoltaics Res. Appl.*, **15** (2007) 659–676.

[107] M. Omastová, M. Trchova, J. Kovarova, and J. Stejskal. Synthesis and Structural Study of Polypyrroles Prepared in the Presence of Surfactants. *Synth. Met.*, **138** (2003) 447–455.

[108] H. Hu, M. Trejo, M. E. Nicho, J. M. Saniger, and A. García-Valenzuela. Adsorption Kinetics of Optochemical NH_3 Gas Sensing with Semiconductor Polyaniline Films. *Sens. Actuators, B, Chem*, **82** (2002) 14–23.

[109] M. Chen. Printed Electrochemical Devices Using Conducting Polymers as Active Materials on Flexible Substrates. *Proc. IEEE*, **93** (2005) 1339 – 1347.

[110] Y. Don Park, J. A. Lim, H. S. Lee, and K. Cho. Interface Engineering in Organic Transistors. *Mater. Today*, **10** (2007) 46–54.

[111] X. Fan, Z. Chu, L. Chen, C. Zhang, F. Wang, Y. Tang, J. Sun, and D. Zou. Fibrous Flexible Solid-Type Dye-Sensitized Solar Cells Without Transparent Conducting Oxide. *Appl. Phys. Lett.*, **92** (2008) 113510–1–3.